

^{60}Fe - ^{60}Ni chronology of core formation in Mars

Haolan Tang,^{1*} † Nicolas Dauphas¹

¹Origins Lab, Department of the Geophysical Sciences and Enrico Fermi Institute, The University of Chicago, 5734 South Ellis Avenue, Chicago IL 60637;

*To whom correspondence should be addressed. E-mail: haolantang@ucla.edu

† Present address: Ion Probe Group, Department of Earth and Space Sciences, University of California, Los Angeles, 595 Charles E. Young Drive East, Los Angeles CA, 90095

5501 words, 5 figures, 1 table

In press in Earth and Planetary Science Letters

January 8, 2014

Abstract

The timescales of accretion, core formation, and magmatic differentiation in planetary bodies can be constrained using extinct radionuclide systems. Experiments have shown that Ni becomes more siderophile with decreasing pressure, which is reflected in the progressively higher Fe/Ni ratios in the mantles of Earth, Mars and Vesta. Mars formed rapidly and its mantle has a high Fe/Ni ratio, so the ^{60}Fe - ^{60}Ni decay system ($t_{1/2}=2.62$ Myr) is well suited to establish the timescale of core formation in this object. We report new measurements of $^{60}\text{Ni}/^{58}\text{Ni}$ ratios in bulk SNC/martian (Shergotty-Nakhla-Chassigny) meteorites and chondrites. The difference in $\epsilon^{60}\text{Ni}$ values between SNC meteorites and the building blocks of Mars assumed to be chondritic (55 % ordinary chondrites +45% enstatite chondrites) is $+0.028\pm 0.023$ (95% confidence interval). Using a model of growth of planetary embryo, this translates into a time for Mars to have reached ~44 % of its present size of $1.9_{-0.8}^{+1.7}$ Myr with a strict lower limit of 1.2 Myr after solar system formation, which agrees with a previous estimate based on ^{182}Hf - ^{182}W systematics. The presence of Mars when planetesimals were still being formed may have influenced the formation of chondrules through bow shocks or by inducing collisions between dynamically excited planetesimals. Constraints on the growth of large planetary bodies are scarce and this is a major development in our understanding of the chronology of Mars.

Key words: Iron-60, accretion, core formation, Mars, age

1. Introduction:

The timescales of accretion, core formation, and mantle differentiation in planetary bodies are key observables that can help us test theories regarding the origin and early evolution of asteroids and planets (see recent reviews by Wadhwa et al., 2006; Dauphas and Chaussidon, 2011). The extinct ^{60}Fe - ^{60}Ni system ($t_{1/2} = 2.62$ Myr; Rugel et al., 2009) is a potentially powerful tool to constrain the timescale of core formation in these bodies because (1) Ni is more siderophile than Fe, therefore the Fe/Ni ratio left in the mantle after core segregation can be strongly fractionated relative to chondrites and (2) core formation in planetesimals and embryos is thought to have occurred within the first several million years of the formation of the solar system, when ^{60}Fe was still extant. Much work has been done previously to estimate the timescales of core formation in various bodies using ^{182}Hf - ^{182}W systematics ($t_{1/2} = 9$ Myr) but ambiguities remain on several aspects of early solar system chronology (see Kleine et al., 2009 for a review). For example, W isotope measurements of SNC (Shergotty-Nakhla-Chassigny) meteorites constrain the time after formation of the solar system for the core of Mars to have reached approximately half of its present size to approximately $1.8_{-1.0}^{+0.9}$ Myr (Dauphas and Pourmand, 2011; Kobayashi and Dauphas, 2013). However, this estimate is really an upper-limit (Mars could have accreted more rapidly than that), as SNC meteorites contain variable excess ^{182}W produced by early silicate differentiation and the accretion timescale was calculated using the least radiogenic ^{182}W values (Kleine et al., 2004a, 2009; Foley et al., 2005). The ^{60}Fe - ^{60}Ni system has seldom been used to constrain early solar system chronology and most studies have focused instead on establishing the initial abundance of ^{60}Fe in meteorites, with important implications for the astrophysical context of solar

system formation. Indeed, high $^{60}\text{Fe}/^{56}\text{Fe}$ ratios obtained by measuring nickel isotopic compositions as well as Fe/Ni ratios by secondary ion mass spectrometers (SIMS) in chondrites were initially taken as fingerprints of the injection of fresh nucleosynthetic products into the solar system by the explosion of a nearby supernova (Tachibana et al., 2003, 2006; Mostefaoui et al., 2004, 2005; Guan et al., 2007; Marhas and Mishra, 2012; Mishra et al., 2010; Mishra and Chaussidon, 2012). Other studies of achondrites and chondritic constituents found lower $^{60}\text{Fe}/^{56}\text{Fe}$ ratios that were interpreted to reflect late disturbance (Chen et al., 2013) or heterogeneous distribution of ^{60}Fe in the early solar system (Sugiura et al., 2006; Quitté et al., 2010, 2011). Recently, Tang and Dauphas (2012) determined by MC-ICPMS the Ni isotopic compositions of bulk angrites, bulk HEDs, bulk chondrites, mineral separates of quenched angrite D'Orbigny, Gujba chondrules, and chondrules and mineral separates from unequilibrated ordinary chondrites (Semarkona and NWA 5717). In all objects analyzed (chondrites and achondrites). They found uniformly low $^{60}\text{Fe}/^{56}\text{Fe}$ ratios corresponding to an initial ratio at the time of condensation of the first solids in the solar nebula (calcium-aluminum-rich inclusions, CAIs) of $(1.15 \pm 0.26) \times 10^{-8}$. Strengthening the case for a uniform $^{60}\text{Fe}/^{56}\text{Fe}$ ratio, they also reported high-precision ^{58}Fe isotope measurements and detected no anomaly in this isotope. The rationale for measuring this isotope of iron is that ^{58}Fe and ^{60}Fe are produced together by neutron captures in supernovae, so any heterogeneity in ^{60}Fe should be accompanied by heterogeneity in ^{58}Fe (Dauphas et al., 2008). The contrapositive of this statement is that ^{58}Fe homogeneity implies ^{60}Fe homogeneity at a level that rules out the highest $^{60}\text{Fe}/^{56}\text{Fe}$ ratios measured by SIMS in chondrules. Spivack-

Birndorf et al. (2012) also concluded that ^{60}Fe was present in low abundance in the early solar system.

The study of Tang and Dauphas (2012) puts ^{60}Fe - ^{60}Ni on solid footings to investigate early solar system chronology. Tang and Dauphas (2012) were thus able to constrain the time of core formation on Vesta to $3.7^{+2.5}_{-1.7}$ Myr after solar system formation, using Ni isotope measurements of HED (Howardite-Eucrite-Diogenite) meteorites. Here, we report Ni isotope measurements of SNC meteorites and chondrites that provide new constraints on the timescale of core formation in Mars.

The dynamical context of Mars' accretion is the subject of much work and speculation. Terrestrial planets are thought to have formed through collisions between Moon to Mars-size planetary embryos over a duration of several tens of million years (Chambers and Wetherill, 1998). Modeling of terrestrial planet formation can reproduce the size and accretion timescale of Earth but the same simulations fail to explain the small size of Mars (Wetherill, 1991; Raymond et al., 2009). One possibility is that Mars grew rapidly into a planetary embryo by accretion of planetesimals and evaded collisions with other embryos during the subsequent stage of chaotic growth, as was experienced by Earth (Chambers and Wetherill, 1998; Chambers, 2004; Kobayashi and Dauphas, 2013). The short accretion timescale of Mars is indeed consistent with this view (Dauphas and Pourmand, 2011). The rapid growth and small mass of Mars can be achieved in the framework of the grand tack scenario, whereby Jupiter migrated inward by type II migration, truncated the inner disk at 1 AU, at which point it entered in a 2:3 resonance with Saturn and started migrating outward (Walsh et al., 2011; Pierens and Raymond, 2011). Accordingly, Mars would have been scattered early on to its present location and

would have stopped growing significantly afterwards. Mars may thus be the sole representative of a generation of planetary bodies that preceded the formation of other terrestrial planets. However, the question of how fast Mars formed remains open because ^{182}Hf - ^{182}W only constrains its accretion to have occurred in the first few million years of solar system formation, a period of time when the solar protoplanetary disk changed rapidly. For example, it was suggested that chondrules could have formed by bow shocks from planetary embryos like Mars (Morris et al., 2012; Boley et al., 2013) but the relative chronology of embryo *vs.* chondrule formation remains uncertain. Refining the chronology of Mars formation is also important for constraining models of embryo growth. Kobayashi and Dauphas (2013) used the mass and accretion time of Mars as constraints in statistical simulations of embryo growth to conclude that Mars most likely formed in a massive disk from relatively small planetesimals, an idea that can be tested further by reducing uncertainties in the growth history of Mars.

In order to establish the timescale of Mars formation using the ^{60}Fe - ^{60}Ni extinct chronometer, we have measured the Ni isotopic compositions of 5 martian (SNC) meteorites and 11 chondrites that are thought to represent the building blocks of Mars. The Ni isotopic results give a timescale of $1.9^{+1.7}_{-0.8}$ Myr for core formation and accretion on Mars, with a robust lower limit of 1.2 Myr.

2. Methodology

2.1 Sample preparation, digestion, and chemical separation

All the chemistry was performed under clean laboratory conditions at the Origins Lab of the University of Chicago. Optima grade HF, reagent grade acetone, and double

distilled HCl and HNO₃ were used for digestion and column chromatography. Millipore Milli-Q water was used for acid dilution. Bulk chondrites were selected to help estimate the Ni isotopic composition of bulk Mars and comprise 5 carbonaceous chondrites (Allende, Murchison, Mighei, Vigarano, Orgueil, Leoville) and 6 H-chondrites (Bath, Bielokrynitschie, Kesen, Kernouvé, Ochansk, Ste. Marguerite). These samples were provided by the Field Museum. The martian meteorites (Shergotty, Chassigny, Nakhla, Zagami, Lafayette) were provided by the Smithsonian Institution. All samples were crushed into powder in an agate mortar before digestion. To assess data quality and make sure that no analytical artifacts were present, terrestrial standards were processed and analyzed together with the meteorite samples.

Sample digestion and chemical separation are described by Tang and Dauphas (2012). Chondrites and martian meteorites weighing 8 to 160 mg were digested in 5-30 ml HF-HNO₃ (in a 2:1 volume ratio) in Teflon beakers placed on a hot plate at ~90 °C for 5-10 days. The solutions were subsequently evaporated to dryness and re-dissolved in a 5-30 mL mixture of concentrated HCl-HNO₃ with a volume ratio of 2:1. For the samples that were not digested completely, the residues were separated by centrifugation and digested in HF-HNO₃ (2:1 volume ratio) and HNO₃ using Parr bombs at 90 °C for 5-10 days until complete digestion. The solutions were dried down and the residues taken back in solution with a minimum amount of concentrated HCl (~11 M) for loading on the first column. In order to obtain sufficiently clean Ni cuts for isotopic measurements, chemical separation of Ni from matrix elements and isobars was done using three steps of liquid chromatography.

U/TEVA cartridge (Horwitz et al., 1992) was used for the first chemistry step to get rid of Ti, Co, Zr and Fe. The column (2 mL volume, 2.5 cm length, 1 cm diameter) was pre-cleaned with 10 mL water, 15 mL 0.4 M HCl, 15 mL 4 M HCl and was then conditioned with 10 mL of concentrated HCl. The sample solution was loaded onto the column in 5-10 mL 10 M HCl. The load solution was collected in clean Teflon beakers and an additional 10 mL of concentrated HCl was passed through the resin and collected in the same beaker. This eluate contained Ni together with Na, Mg, Ca and other matrix elements. After drying down, the Ni elution cut from the first column chemistry was re-dissolved in 5 mL of a mixture of 20 % 10 M HCl-80 % acetone (by volume) and loaded onto 5 mL (40 cm length, 0.4 cm diameter) pre-cleaned Bio-Rad AG50-X12 200-400 mesh hydrogen-form resin in a Teflon column, previously conditioned with 10 mL 20 % 10 M HCl-80 % acetone. After loading the sample solution and rinsing with 30 mL 20 % 10 M HCl – 80% acetone mixture to eliminate Cr and any remaining Fe, Ni was collected by eluting 150 mL of the HCl-acetone mixture into a jar containing 30 mL H₂O to dilute HCl and stabilize Ni in the eluate. In those conditions, Mg, Na, Ca, and other matrix elements were retained on the resin (Strelow et al., 1971; Tang and Dauphas, 2012). The collected Ni solution was evaporated at moderate temperature (<90 °C) under a flow of N₂ to avoid the formation of organic complexes with acetone and accelerate evaporation. After evaporation, the Ni fraction was dissolved in 1 mL of aqua regia (1:3 HNO₃:HCl) to remove any organic residue formed during evaporation. This HCl-acetone column was repeated five times to ensure thorough separation of major rock forming element Mg from Ni, two elements that are notoriously difficult to separate. Zinc is a significant interference on low abundance isotope ⁶⁴Ni. It was removed using a third column filled

with 1 mL (2 cm length, 0.8 cm diameter) Bio-Rad AG1W-X8 anionic ion exchange resin in 8 M HBr medium (Moynier et al., 2006). Nickel was eluted in 8 mL 8 M HBr, whereas Zn was retained on the resin.

The entire procedural blanks were ~35 ng for Ni isotope composition measurements, negligible compared to the amounts of Ni in the samples. Nickel yield of the entire procedure was 90-100 %.

2.2 Mass spectrometry

All measurements were performed at the Origins Laboratory of the University of Chicago using a Neptune MC-ICPMS equipped with an OnTool Booster 150 (Pfeiffer) interface jet pump. Jet sampler and X skimmer cones were used. The samples were re-dissolved in 0.3 HNO₃ and introduced into the mass spectrometer with Ar + N₂ using an Aridus II desolvating nebulizer at an uptake rate of ~ 100 µL/min. The instrument sensitivity for ⁵⁸Ni was 100 V/ppm. One analysis consisted of 25 cycles, each acquisition lasting for 8.4 s. During a session, each sample solution was measured 13 times bracketed by SRM 986. A small isobaric interference from the least abundant isotope of iron, ⁵⁸Fe, on the most abundant isotope of nickel, ⁵⁸Ni, was corrected by monitoring ⁵⁷Fe (the ⁵⁸Fe/⁵⁸Ni ratio was always less than 0.00005 in our measurements). All isotopes were measured with Faraday cups with 10¹¹ Ω resistance amplifiers. Background was subtracted using an on-peak zero procedure. Internal normalization was used to correct mass-dependent isotopic fractionation by fixing ⁶¹Ni/⁵⁸Ni to 0.016720 or ⁶²Ni/⁵⁸Ni to 0.053389 (Gramlich et al., 1989) using the exponential law (Maréchal et al., 1999).

In the following, we only discuss results based on the normalization to $^{61}\text{Ni}/^{58}\text{Ni}$ because: (1) it reduces the spread in $\epsilon^{60}\text{Ni}$ values of chondrites (Table 1) arising from the presence of nucleosynthetic anomalies on Ni isotopes and (2) although Ti in the samples have been eliminated completely, there is still a potential interference on ^{62}Ni coming from titanium oxide ($^{46}\text{Ti}^{16}\text{O}$) in the acid background (Tang and Dauphas, 2012).

Approximately 20-25 % of the original sample solutions were kept as safety aliquots and for Fe/Ni ratio measurements by MC-ICPMS using both the bracketing and standard addition techniques (see Tang and Dauphas 2012 for details). The standard addition method largely eliminates possible matrix effects in elemental analyses (*e.g.*, Harris, 2011). The Fe/Ni ratios measured by standard addition were compared with Fe/Ni ratios measured by simple sample-standard bracketing and the values were identical within uncertainties. Fe/Ni ratios in terrestrial standards were all within 3 % of their reference values, demonstrating the accuracy of our measurements.

The uncertainties on Fe and Ni concentrations are those given by Isoplot for the x -intercept of the standard addition data. Fe/Ni ratios in Table 1 were obtained by the standard addition technique.

3. Results

Table 1 shows the Ni isotopic compositions and Fe/Ni ratios measured in meteorites and terrestrial rock standards. Below, we focus our discussion on results reported using $^{61}\text{Ni}/^{58}\text{Ni}$ internal normalization. Terrestrial standards passed through the same column chemistry as meteoritic samples have normal Ni isotopic ratios, attesting to the accuracy of the measurements. Note that ^{64}Ni was not measured in several samples with very low Ni contents (BE-N, BHVO-2, DNC-1, and all SNC meteorites).

The Ni isotope measurements of bulk chondrites agree well with previous studies reporting the presence of small isotopic anomalies of nucleosynthetic origin for Ni isotopes in meteorites (Dauphas et al., 2008; Regelous et al., 2008; Steele et al., 2012). $\epsilon^{62}\text{Ni}$ and $\epsilon^{64}\text{Ni}$ isotopic anomalies in chondrites are correlated with each other (Fig. 1). Steele et al. (2012) measured the Ni isotopic composition of meteoritic materials using a double spike technique and concluded that the cause of ^{62}Ni and ^{64}Ni isotopic variations was most likely variations in the neutron-poor isotope ^{58}Ni , which the authors ascribed to incomplete mixing of products of supernova nucleosynthesis in the solar protoplanetary disk. $\epsilon^{62}\text{Ni}$ and $\epsilon^{64}\text{Ni}$ are also correlated with $\epsilon^{54}\text{Cr}$ anomalies (Fig. 2A; $\epsilon^{54}\text{Cr}=7.430\times\epsilon^{62}\text{Ni}+0.055$), the carrier of which has been identified as ^{54}Cr -rich nanooxide/nanospinels of supernova origin (Dauphas et al, 2010; Qin et al., 2011). More work is needed to identify the presolar carrier of Ni isotopic anomalies in meteorites. $\epsilon^{60}\text{Ni}$ values in chondrites also show departure from terrestrial composition. These variations in the ^{60}Ni isotopic composition of bulk chondrites are unlikely to be related to ^{60}Fe because all bulk chondrites have similar Fe/Ni ratios yet distinct $\epsilon^{60}\text{Ni}$ values, which is impossible to explain if the $^{60}\text{Fe}/^{56}\text{Fe}$ ratio was uniform (Tang and Dauphas, 2012). Furthermore, samples with low $\epsilon^{60}\text{Ni}$ have normal $\epsilon^{58}\text{Fe}$, indicating a decoupling between variations in ^{60}Ni isotopic anomalies and neutron-rich isotopes ^{58}Fe and ^{60}Fe . Isotopic anomalies in ^{60}Ni do not correlate with ^{62}Ni or ^{64}Ni , calling for the presence of a third nucleosynthetic component in the solar system Ni isotope mix.

Within the general groups of ordinary and enstatite chondrites, the different samples have uniform Ni isotopic compositions. Combining the results presented in Table 1 and Figure 3 with previously published data (Dauphas et al., 2008; Regelous et al., 2008;

Steele et al., 2012), we estimate the weighted average $\epsilon^{60}\text{Ni}$ isotopic values of ordinary and enstatite chondrites to be -0.048 ± 0.008 (n=13) and -0.019 ± 0.010 (n=5), respectively (see Table S1 in Appendix B for a compilation). All uncertainties are 95 % confidence intervals of the averages and were calculated using the Isoplot software.

Regardless of the variability in ^{142}Nd and ^{182}W anomalies among SNC meteorites (Kleine et al., 2004a, 2009; Foley et al., 2005), the Ni isotopic composition of five SNC meteorites (Shergotty, Chassigny, Nakhla, Zagami, Lafayette) is constant and identical to the terrestrial value (Fig. 3). No correlation is found between the Ni isotopic composition and Fe/Ni ratios of the different SNC meteorites (Fig. 4). The weighted average $\epsilon^{60}\text{Ni}$ value of SNC meteorites is -0.010 ± 0.022 (MSWD=0.034).

4. Discussion

Angrites and HED meteorites show variations in $\epsilon^{60}\text{Ni}$ linearly correlated with Fe/Ni ratio, indicating global silicate differentiation while ^{60}Fe was still alive. In contrast, the uniform $\epsilon^{60}\text{Ni}$ value found in all SNC meteorites, indicates that the magmatic differentiation events that fractionated Fe/Ni ratios in SNC meteorites must have taken place after ^{60}Fe had fully decayed. The inferred initial ratio of $(-0.01 \pm 1.19) \times 10^{-9}$ at the time when Fe-Ni system was closed translates into a minimum age for Fe/Ni fractionation of 8.6 Myr after solar system formation, assuming $(^{60}\text{Fe}/^{56}\text{Fe})_0 = (1.15 \pm 0.26) \times 10^{-8}$ as the initial ratio at the time of CAI formation (Fig. 4; Tang and Dauphas, 2012). This timescale is fully consistent with the ~40-100 Myr formation interval for the shergottite mantle sources, as derived from coupled $^{142,143}\text{Nd}$ systematics (Foley et al., 2005, Caro et al., 2008, Debaille et al., 2007), and with the 2-stage ^{146}Sm - ^{142}Nd model age for the nakhlites-Chassigny group of ~25 Myr (Harper et al.,

1995, Foley et al., 2005). Some of the Fe/Ni fractionation recorded in SNC meteorites must reflect mineral/melt fractionation during partial melting of the martian mantle and subsequent differentiation of the magmas, which took place at least 0.5 Gyr after solar system formation (Lapen et al., 2010), well after complete decay of ^{60}Fe . On the other hand, both the terrestrial and martian mantles are known to host heterogeneities in decay products of short-lived nuclides ^{146}Sm and ^{182}Hf (Harper et al., 1995; Lee and Halliday, 1997; Jagoutz et al., 2003; Kleine et al., 2004a; Foley et al., 2005; Caro et al., 2008; Debaille et al., 2007; Willbold et al., 2011; Touboul et al., 2012). No such heterogeneity was found for ^{60}Fe - ^{60}Ni in the martian or terrestrial mantles. The average $\epsilon^{60}\text{Ni}$ of all SNC meteorites measured in this study is taken as representative of the $\epsilon^{60}\text{Ni}$ value of the bulk Martian mantle ($\epsilon^{60}\text{Ni} = -0.010 \pm 0.022$).

The time of core formation on Mars has previously been estimated using the ^{182}Hf - ^{182}W chronometer. A difficulty however is that different martian meteorites have variable $\epsilon^{182}\text{W}$ and $\epsilon^{142}\text{Nd}$ values, reflecting early Hf/W and Sm/Nd fractionation presumably associated with magma ocean crystallization (Kleine et al., 2004a, 2009; Foley et al., 2005). The $\epsilon^{182}\text{W}$ values in SNC meteorites range from +0.3 to +3 (Foley et al., 2005; Kleine et al., 2004a, 2009), the highest values being characteristic of Nakhrites that are more enriched and oxidized than other SNC meteorites and may bear the signature of a crustal component. Conservatively, one can use the lowest $\epsilon^{182}\text{W}$ of $+0.4 \pm 0.2$ measured in Shergottites and the Hf/W ratio of the martian mantle (3.51 ± 0.45 ; Dauphas and Pourmand, 2011) to estimate the age for core formation on Mars. Using this approach, Dauphas and Pourmand (2011) estimated that Mars accreted approximately 44 % of its present mass in $1.8^{+0.9}_{-1.0}$ Myr. As discussed in the introduction, this value is really an

upper-limit, as the ^{182}W isotopic composition of the martian mantle could be more radiogenic than $\varepsilon^{182}\text{W}=+0.4 \pm 0.2$.

The Hf-W approach takes advantage of the fact that core formation led to a drastic fractionation of Hf and W, as Hf is strongly lithophile and W is moderately siderophile. Similarly, core formation in the terrestrial planets fractionated Fe from Ni in the silicate mantle. If Mars' core formed early, while ^{60}Fe was still alive, the high Fe/Ni ratio of the martian mantle should have produced excess radiogenic ^{60}Ni relative to bulk Mars, taken to be chondritic. The ingredients to calculate a timescale of core formation on Mars are the Fe/Ni ratios and $\varepsilon^{60}\text{Ni}$ values of the mantle of Mars and chondrites.

The $\varepsilon^{60}\text{Ni}$ value of the martian mantle is that obtained here from measurements of SNC meteorites, *i.e.*, $\varepsilon^{60}\text{Ni}_{\text{mantle}} = -0.010 \pm 0.022$ (the error bar is the 95 % confidence interval of the weighted mean). The Fe/Ni ratio of the bulk mantle of Mars cannot be measured directly in SNC meteorites because Fe and Ni could be fractionated during melting and crystallization after ^{60}Fe was extinct. Instead, the Fe/Ni ratio of the bulk mantle of Mars was estimated by Warren (1999) based on MgO-NiO and MgO-FeO correlations to be ~ 350 , which corresponds to a $^{56}\text{Fe}/^{58}\text{Ni}$ ratio of ~ 472 (also see Wänke and Dreibus, 1988).

As discussed in Sect. 3, chondrites show variations in Ni isotopic ratios (not only $\varepsilon^{60}\text{Ni}$ but also $\varepsilon^{62}\text{Ni}$ and $\varepsilon^{64}\text{Ni}$) that cannot be ascribed to radiogenic ingrowth but must reflect instead the presence of planetary scale nucleosynthetic anomalies, as has been documented previously for other elements such as Mo (Dauphas et al., 2002a, b; Burkhardt et al., 2011). In order to estimate the $\varepsilon^{60}\text{Ni}$ value of bulk Mars, one must know the nature of the building blocks that made Mars. The average $\Delta^{17}\text{O}$, $\varepsilon^{50}\text{Ti}$, $\varepsilon^{54}\text{Cr}$, $\varepsilon^{62}\text{Ni}$,

and $\epsilon^{92}\text{Mo}$ values of carbonaceous (CC), ordinary (OC), and enstatite (EC) chondrites are compiled in Figure 2 (Cr: Qin et al., 2010; Trinquier et al., 2007; Ti: Trinquier et al. 2009; Zhang et al., 2012; Mo: Dauphas et al., 2002a, b; Burkhardt et al., 2011; Ni: Dauphas et al., 2008; Steele et al., 2012; Tang and Dauphas, 2012; O: Clayton et al., 1983, 1984, 1991, 1999; Weisberg et al., 2001; Tables S1-S5). Warren (2011) showed that in any case, carbonaceous chondrites contributed less than 18 %. The mixture advocated by Sanloup et al. (1999) (55 % H + 45 % EH) can reproduce the $\Delta^{17}\text{O}$, $\epsilon^{50}\text{Ti}$, $\epsilon^{54}\text{Cr}$, $\epsilon^{62}\text{Ni}$, and $\epsilon^{92}\text{Mo}$ values measured in SNC meteorites while that of Lodders and Fegley (1997) does not (85 % H + 11 % CV + 4 % CI; Fig. 2). Therefore, the bulk $\epsilon^{60}\text{Ni}$ isotopic composition of Mars is calculated using the following equation:

$$\epsilon^{60}\text{Ni}_{\text{Bulk Mars}} = (\epsilon^{60}\text{Ni}_{\text{OC}}X_{\text{H}}[\text{Ni}]_{\text{H}} + \epsilon^{60}\text{Ni}_{\text{EC}}X_{\text{EH}}[\text{Ni}]_{\text{EH}})/(X_{\text{H}}[\text{Ni}]_{\text{H}} + X_{\text{EH}}[\text{Ni}]_{\text{EH}}) \quad (2),$$

where X is the weight fraction of the various chondrite types in bulk Mars (55% H+45% EH; Sanloup et al., 1999) and [Ni] is the Ni concentration (Wasson and Kallemeyn, 1988). For $\epsilon^{60}\text{Ni}$, we take the average values for OC and EC as proxies for H and EH because meteorites within these groups have uniform Ni isotopic compositions. The resulting Ni isotopic composition of bulk Mars is $\epsilon^{60}\text{Ni} = -0.038 \pm 0.006$. Using the mixing proportions proposed by Lodders and Fegley (1997), the $\epsilon^{60}\text{Ni}$ value of bulk Mars would have been -0.056 ± 0.008 , which is slightly lighter than the value adopted here. The Fe/Ni ratio of bulk Mars is calculated using the compilation of Wasson and Kallemeyn (1988) and the following mass-balance equation (55 % H+45 % EH):

$$\left(\frac{\text{Fe}}{\text{Ni}}\right)_{\text{Bulk Mars}} = \left[\left(\frac{\text{Fe}}{\text{Ni}}\right)_{\text{H}} X_{\text{H}}[\text{Ni}]_{\text{H}} + \left(\frac{\text{Fe}}{\text{Ni}}\right)_{\text{EH}} X_{\text{EH}}[\text{Ni}]_{\text{EH}}\right]/(X_{\text{H}}[\text{Ni}]_{\text{H}} + X_{\text{EH}}[\text{Ni}]_{\text{EH}}). \quad (3)$$

The Fe/Ni ratio of bulk Mars is therefore 17.0. The Fe/Ni ratio of the Martian core is not known directly but can be obtained by mass-balance,

$$\left(\frac{\text{Fe}}{\text{Ni}}\right)_{\text{Mars core}} = \frac{(\text{Fe}/\text{Ni})_{\text{Bulk Mars}}[\text{Ni}]_{\text{Bulk Mars}}M_{\text{Bulk Mars}} - (\text{Fe}/\text{Ni})_{\text{Mars mantle}}[\text{Ni}]_{\text{Mars mantle}}M_{\text{Mars mantle}}}{[\text{Ni}]_{\text{Bulk Mars}}M_{\text{Bulk Mars}} - [\text{Ni}]_{\text{Mars mantle}}M_{\text{Mars mantle}}}. \quad (4)$$

This yields a Fe/Ni ratio for Mars' core of 9.79.

To translate Ni isotope measurements of SNC meteorites into age constraints, a proper model of core formation must be used. A reasonable assumption to make is that core formation tracks planetary accretion, meaning that whenever mass is added to Mars, metal is removed into the core in proportion to the present core/mantle ratio. To parameterize the growth of Mars, Dauphas and Pourmand (2011) used some formalism relevant to oligarchic growth of embryos from planetesimals (Thommes et al., 2001; Chambers, 2006),

$$\frac{M_{\text{Mars}}(t)}{M_{\text{Mars}}} = \tanh^3(t/\tau), \quad (5)$$

where t is counted from the formation of the solar system, and τ is the accretion timescale. At $t = \tau$, the size of embryo is $\tanh^3(1) = 44\%$ of its present size. More recently, Kobayashi and Dauphas (2013) and Morishima et al. (2013) used more realistic model simulations (statistical or N-body) to investigate the influence of the accretion history of Mars on ^{182}Hf - ^{182}W model age. Much can be learned from these sophisticated simulations but the formalism used by Dauphas and Pourmand (2011) captures the most salient features of embryo growth in a single parameter (τ), so this formalism is used here.

Another point that deserves consideration is the question of knowing whether metal in the incoming bodies was able to equilibrate fully with the whole mantle of protoMars (Halliday, 2004; Nimmo and Agnor, 2006; Kleine et al., 2004b; 2009; Nimmo et al., 2010; Rudge et al., 2010; Dahl and Stevenson, 2010; Deguen et al., 2011). At one extreme, one could imagine a model whereby no equilibration occurs and the metal of the incoming bodies sinks directly to the core, without exchange with the mantle. In this

situation, the ^{60}Fe - ^{60}Ni system would record the time of core formation in the building blocks of Mars, not core formation in Mars itself. Such scenarios have been considered for Earth because chaotic growth is thought to take place through the collisions of large bodies (Chambers and Wetherill, 1998, Raymond et al., 2009). For example, the Moon is thought to have formed by the impact with the protoEarth of an embryo the size of Mars or possibly half the size of Earth (Cameron and Ward, 1976; Canup, 2012; Canup and Asphaug, 2001; Ćuk and Stewart, 2012; Hartmann and Davis, 1975; Reufer et al., 2012). The degree to which terrestrial ^{182}Hf - ^{182}W isotope systematics is affected by such large impacts is still debated. For Mars, the situation is easier than for Earth as evidence suggests that this planet formed very rapidly from the accretion of small planetesimals (Walsh et al., 2011; Dauphas and Pourmand, 2011; Kobayashi and Dauphas, 2013). Morishima et al. (2013) evaluated how lack of equilibration between impactor-core and target-mantle could influence the accretion timescale of Mars inferred from ^{182}Hf - ^{182}W systematics and they concluded that the effect was small and that Mars formed rapidly. Rapid accretion means that there was enough ^{26}Al for both Mars and the incoming bodies to be extensively molten (Grimm and McSween, 1993; Dauphas and Pourmand, 2011), favoring efficient mixing. Furthermore, the small size of the accreting planetesimals means that they were vaporized upon impact, allowing equilibration with the target mantle (Nimmo and Agnor, 2006). Their small sizes also allowed sinking metal to break down into droplets of size around 20 cm that could have easily equilibrated with the surrounding medium (Rubie et al., 2003; Samuel, 2012; Deguen et al., 2011). Accordingly, we assume complete ^{60}Fe - ^{60}Ni equilibration between incoming planetesimals and the mantle of proto-Mars.

Halliday et al. (1996), Harper and Jacobsen (1996), and Jacobsen (2005) developed models to calculate the isotopic evolution of ^{182}W in planetary bodies for different accretion timescales. The equations given in these papers incorporate the fact that the core does not contain any of the parent nuclide ^{182}Hf . This assumption is not valid for ^{60}Fe - ^{60}Ni systematics because the core of Mars would have been an important repository of ^{60}Fe and the equations have to be modified accordingly (Appendix A):

$$\varepsilon^{60}\text{Ni}_{\text{Mars mantle}}(t) - \varepsilon^{60}\text{Ni}_{\text{Chondrite}}(t) = \lambda f_m q_{\text{Ni}} \left(\frac{^{60}\text{Fe}}{^{56}\text{Fe}} \right)_{\text{Chondrite},0} \int_0^t \left[\frac{M(x)}{M(t)} \right]^{1-\frac{f_m}{f_c}} e^{-\lambda x} dx \quad (6)$$

Using the parameterization for embryo growth given in Eq. 5, this equation takes the form,

$$\begin{aligned} \varepsilon^{60}\text{Ni}_{\text{Mars mantle}}(t) - \varepsilon^{60}\text{Ni}_{\text{Chondrite}}(t) \\ = \lambda f_m q_{\text{Ni}} \left(\frac{^{60}\text{Fe}}{^{56}\text{Fe}} \right)_{\text{Chondrite},0} \int_0^t \left[\frac{\tanh(x/\tau)}{\tanh(t/\tau)} \right]^{3(1-\frac{f_m}{f_c})} e^{-\lambda x} dx \quad (7) \end{aligned}$$

Where $q_{\text{Ni}} = 10^4 (^{56}\text{Fe}/^{60}\text{Ni})_{\text{Chondrite}} = 595525$ (Wasson and Kallemeyn, 1988) and $\varepsilon^{60}\text{Ni}_{\text{Chondrite}}(\text{present}) = -0.038 \pm 0.006$ (this study, Steele et al., 2012; Tang and Dauphas, 2012) assuming that Mars is made of 55 % OC+ 45 % EC; $(^{60}\text{Fe}/^{56}\text{Fe})_{\text{Chondrite},0} = (1.15 \pm 0.26) \times 10^{-8}$ at CAI formation (Tang and Dauphas, 2012); $\varepsilon^{60}\text{Ni}_{\text{Mars mantle}}(\text{present}) = -0.010 \pm 0.022$ (this study; Table 1); $\lambda = 0.26456 \text{ Myr}^{-1}$ is the decay constant of ^{60}Fe ; $f_m = (\text{Fe}/\text{Ni})_{\text{Mars mantle}} / (\text{Fe}/\text{Ni})_{\text{Chondrite}} - 1 = 19.38$; $f_c = (\text{Fe}/\text{Ni})_{\text{Mars core}} / (\text{Fe}/\text{Ni})_{\text{Chondrite}} - 1 = -0.430$.

In Fig. 5, the difference $\varepsilon^{60}\text{Ni}_{\text{Mars mantle}}(t) - \varepsilon^{60}\text{Ni}_{\text{Chondrite}}(t)$ is plotted as a function of time for different accretion timescales. If Mars had formed very rapidly at the time of CAI formation ($\tau=0 \text{ Myr}$), then excess $\varepsilon^{60}\text{Ni}$ of the bulk martian mantle relative to chondrites should have been +0.14. Conversely, if Mars' core had formed after complete

decay of ^{60}Fe , then there should not have been any excess ^{60}Ni . The measured difference $\varepsilon^{60}\text{Ni}_{\text{Mars mantle}}(\text{present}) - \varepsilon^{60}\text{Ni}_{\text{Chondrite}}(\text{present}) = +0.028 \pm 0.023$ translates into an accretion timescale of $1.9_{-0.8}^{+1.7}$ Myr. The error bar on τ is the 95 % confidence interval calculated by propagating uncertainties on all model parameters using a Monte-Carlo approach. The upper-bound is loosely defined because the $\varepsilon^{60}\text{Ni}$ value of SNC meteorites is barely resolvable from that of chondrites. However, the lower bound of 1.2 Myr after CAI formation is a firm limit. Indeed, any accretion timescale lower than that would have produced enough radiogenic ^{60}Ni in the martian mantle to be readily detected by our technique.

The timescale obtained for Mars core formation and accretion of $1.9_{-0.8}^{+1.7}$ Myr after CAI formation agrees with the previous value of $1.8_{-1.0}^{+0.9}$ Myr based on ^{182}Hf - ^{182}W systematics of SNC meteorites (Dauphas and Pourmand, 2011). As discussed previously, the timescale obtained using ^{182}Hf - ^{182}W systematics is strictly speaking an upper-limit. On the other hand, ^{60}Fe - ^{60}Ni systematics provides a solid lower limit on the accretion timescale of Mars. Combining the two estimates, we obtain $1.8_{-0.6}^{+0.8}$ Myr. This means that Mars had reached approximately 44 % of its present size by ~ 1.8 Myr, a time when ^{26}Al was still alive and provided sufficient heat to melt planetary bodies including Mars.

The new constraint on the accretion timescale of Mars can help put its formation in the broader context of early solar system evolution. Application of ^{182}Hf - ^{182}W systematics to magmatic iron meteorites indicates that most of them were segregated as metallic cores from their parent-bodies within approximately ~ 1 Myr of the formation of the solar system (Kleine et al., 2005, 2009; Schersten et al., 2006; Markowski et al., 2006; Qin et al., 2008; Burkhardt et al., 2012; Kruijer et al., 2012; Wittig et al., 2013). At that time,

^{26}Al was a potent heat source, explaining why all the remnants from this early stage of planetesimal formation are differentiated (*i.e.*, molten) meteorites. Planetesimal formation was a protracted phenomenon that continued at least until ~ 3 Myr after CAI formation (Kita et al., 2005; Villeneuve et al., 2009; Dauphas and Chaussidon 2011 and references therein). The planetesimals from that period are mostly undifferentiated because ^{26}Al had decayed to a too low level to induce significant melting. A conclusion of the present study is that Mars would have accreted while planetesimals were still forming. By the time of chondrite formation, Mars would have already reached almost its full size, raising the possibility of forming chondrules by bow shocks generated by embryos (Morris et al., 2012; Boley et al., 2013) or by collisions between planetesimals (Asphaug et al., 2011; Sanders and Scott, 2012; Fedkin and Grossman, 2013) that would have been dynamically excited by the presence of an embryo.

A similar approach to that used for Mars or Vesta cannot be applied to Earth because its accretion timescale was undoubtedly too long for ^{60}Fe decay to impart any variation in the isotopic composition of ^{60}Ni in the terrestrial mantle. Furthermore, at high pressure and high temperature Ni tends to become more lithophile (Thibault and Walter, 1995; Li and Agee, 1996; Ito et al., 1998), so the Fe/Ni ratio in Earth's mantle is too close to the chondritic ratio to yield any useful constraints on the accretion timescale of Earth.

5. Conclusion

The ^{60}Fe - ^{60}Ni extinct radionuclide system can provide constraints on the timing of core formation in early-formed planetary bodies. Using a new estimate of the initial $^{60}\text{Fe}/^{56}\text{Fe}$ ratio of $(1.15 \pm 0.26) \times 10^{-8}$ in the solar system, we present the first chronological application of the ^{60}Fe - ^{60}Ni decay system to establish the timescale of accretion and core

segregation in Mars. The inferred timescale of $1.9_{-0.8}^{+1.7}$ Myr after condensation of the first solids agrees with a value of $1.8_{-1.0}^{+0.9}$ Myr obtained using the ^{182}Hf - ^{182}W decay system. However, this last estimate was strictly speaking an upper-limit, while ^{60}Fe - ^{60}Ni provides a very robust lower limit. The two approaches are thus complementary.

The short accretion timescale obtained for Mars indicates that it grew while planetesimals were still being accreted. Most simulations of embryo growth start by considering a disk populated by already formed planetesimals, an assumption that should be relaxed in light of our results. The presence of an embryo when planetesimals were still being formed may have influenced the formation of chondrules through bow shocks or by inducing collisions between dynamically excited planetesimals.

Constraints on the accretion timescale of planets are hard to come by and the successful application of ^{60}Fe - ^{60}Ni to Mars accretion and differentiation is a major advance in our understanding of early solar system chronology.

Acknowledgements.

This work was supported by grants from the NASA Cosmochemistry (NNX12AH60G) and NSF (EAR1144429) programs. The samples were generously provided by the Robert A. Pritzker Center for Meteoritics at the Field Museum (Philipp R. Heck) and Smithsonian National Museum of Natural History (Timothy J. McCoy). Discussions with Hiroshi Kobayashi, Alessandro Morbidelli, Mark Fornace, and Robert

N. Clayton were greatly appreciated. This manuscript benefited from the comments of two anonymous reviewers.

Figure caption:

Fig. 1. Nickel isotope compositions of iron and chondritic meteorites analysed by Steele et al. (2012) (open symbols), Dauphas et al. (2008) and this study (filled symbols).

Fig. 2. Isotopic anomalies in chondrites and SNC meteorites: (A) $\epsilon^{62}\text{Ni}$ vs. $\epsilon^{54}\text{Cr}$; (B) $\epsilon^{62}\text{Ni}$ vs. $\Delta^{17}\text{O}$, (C) $\epsilon^{62}\text{Ni}$ vs. $\epsilon^{50}\text{Ti}$, and (D) $\epsilon^{62}\text{Ni}$ vs. $\epsilon^{92}\text{Mo}$ (Cr: Qin et al., 2010; Trinquier et al., 2007; Ti: Trinquier et al. 2009; Zhang et al., 2012; Ni: Steele et al., 2012; Tang and Dauphas, 2012; O: Clayton et al., 1983, 1984, 1991, 1999; Weisberg et al., 2001; Mo: Dauphas et al., 2002a, b; Burkhardt et al., 2011). Proposed model compositions of bulk Mars are also shown (85 % H+11 % CV+4 % CI; Lodders and Fegley, 1997; 55 % H+45 % EH, Sanloup et al., 1999). Only the model of Sanloup et al. (1999) can reproduce the isotopic anomalies measured in SNC meteorites. In all the panels, terrestrial composition is at (0,0) coordinate.

Fig. 3. $\epsilon^{60}\text{Ni}$ values in terrestrial standards (black cycles), chondrites (diamonds), and Martian meteorites (open squares) (Table 1; Steele et al., 2012; Dauphas et al., 2008; Tang and Dauphas, 2012). Ni isotopic ratios are reported in the ϵ -notation; $\epsilon^{60}\text{Ni} = [({}^{60}\text{Ni}/{}^{58}\text{Ni})_{\text{sample}} / ({}^{60}\text{Ni}/{}^{58}\text{Ni})_{\text{standard}} - 1] \times 10^4$, where ${}^{60}\text{Ni}/{}^{58}\text{Ni}$ ratios have been corrected for natural and laboratory-introduced mass fractionation by internal normalization to a constant ${}^{61}\text{Ni}/{}^{58}\text{Ni}$ ratio. The error bars represent 95 % confidence intervals. The gray bars represent the weighted averages of chondrites. According to the mixing model described in the text (Sanloup et al., 1999), SNC values for $\Delta^{17}\text{O}$, $\epsilon^{50}\text{Ti}$, $\epsilon^{54}\text{Cr}$, $\epsilon^{62}\text{Ni}$, and $\epsilon^{92}\text{Mo}$ can be reproduced with 55% ordinary chondrites (OC), and 45% enstatite chondrites (EC), corresponding to a bulk Mars $\epsilon^{60}\text{Ni}$ value of -0.038 ± 0.006 . All

SNC meteorites analyzed in this study have terrestrial $\epsilon^{60}\text{Ni}$ values, averaging -0.010 ± 0.022 (red bar and red square). This is taken to be the isotopic composition of the Martian mantle (see text for details).

Fig. 4. ^{60}Fe - ^{60}Ni diagram of Martian meteorites (see Fig. 3 caption for notations). In $\epsilon^{60}\text{Ni}$ vs. $^{56}\text{Fe}/^{58}\text{Ni}$ isochron diagram, the intercept gives the initial Ni isotopic composition $\epsilon^{60}\text{Ni}_0$, while the slope is proportional to the initial $^{60}\text{Fe}/^{56}\text{Fe}$ ratio; slope = $25,961 \times (^{60}\text{Fe}/^{56}\text{Fe})_0$. No correlation was found between $\epsilon^{60}\text{Ni}$ vs. $^{56}\text{Fe}/^{58}\text{Ni}$ in Martian meteorites (open squares). The average $\epsilon^{60}\text{Ni}$ (-0.010 ± 0.022) value in SNC meteorites is taken to be representative of the Martian mantle (red square). The model isochron defined by the bulk martian mantle (SNC meteorites, red square) and bulk Mars (chondrites, green dot) gives an initial $^{60}\text{Fe}/^{56}\text{Fe}$ ratio of 2.5×10^{-5} .

Fig. 5. $\epsilon^{60}\text{Ni}$ isotope evolution of the mantle of Mars ($^{58}\text{Fe}/^{56}\text{Ni} = 472$; Warren et al., 1999) for different accretion timescales (τ) of Mars; $M_{\text{Mars}} = M_{\text{Final}} \times \tanh^3(t/\tau)$. The x-axis is the time (t) after solar system formation defined as CAI condensation. $\epsilon^{60}\text{Ni}$ isotopic composition in Martian mantle remains constant after 10 Myr within our uncertainty due to complete decay of ^{60}Fe . The Ni isotopic composition of SNC meteorites (red dot) constrains the accretion timescale of Mars to be $1.9_{-0.8}^{+1.7}$ Myr.

Appendix A: Modeling the ^{60}Ni isotopic evolution of the mantle of a growing planet

The following notations are used:

- $\varepsilon^{60}\text{Ni}_i = [({}^{60}\text{Ni}/{}^{58}\text{Ni})_i / ({}^{60}\text{Ni}/{}^{58}\text{Ni})_{\text{std}} - 1] \times 10,000$,
- M_m , M_c , and $M = M_m + M_c$ are the masses of the mantle, core, and whole planet, respectively,
- $[\text{E}]_m$, $[\text{E}]_c$, and $[\text{E}]_{m \rightarrow c}$ are the concentrations of element/isotope E in the mantle, core, and mass-flux from mantle to core, respectively,
- $\gamma = M_c / (M_m + M_c)$,
- $D^{\text{E}} = [\text{E}]_{\text{metal}} / [\text{E}]_{\text{silicate}}$,
- $f_m = (\text{Fe}/\text{Ni})_m / (\text{Fe}/\text{Ni})_{\text{CHUR}} - 1$ and $f_c = (\text{Fe}/\text{Ni})_c / (\text{Fe}/\text{Ni})_{\text{CHUR}} - 1$,
- $R = {}^{60}\text{Ni} / {}^{58}\text{Ni}$.

We start by writing the following equation governing the concentration of Fe in the mantle,

$$d(M_m[\text{Fe}]_m) = [\text{Fe}]_{\text{CHUR}}d(M_m + M_c) - [\text{Fe}]_{m \rightarrow c}dM_c. \quad (A1)$$

The metal that is removed is in equilibrium with the silicate at each time step and we have,

$$(1 - \gamma)d(M[\text{Fe}]_m) = [\text{Fe}]_{\text{CHUR}}dM - \gamma D^{\text{Fe}}[\text{Fe}]_m dM. \quad (A2)$$

After some rearrangement, it follows,

$$d[\text{Fe}]_m = \frac{1}{1 - \gamma} \{ [\text{Fe}]_{\text{CHUR}} - (1 - \gamma + \gamma D^{\text{Fe}})[\text{Fe}]_m \} d \ln M. \quad (A3)$$

With the initial condition that at the beginning of accretion, bulk metal must be in equilibrium with bulk silicate, we find that the concentrations in the mantle (and by mass-balance the core) must remain constant throughout accretion if γ and D^{Fe} remain constant,

$$[\text{Fe}]_m = [\text{Fe}]_{\text{CHUR}} / (1 - \gamma + \gamma D^{\text{Fe}}), \quad (\text{A4})$$

$$[\text{Fe}]_c = D^{\text{Fe}} [\text{Fe}]_{\text{CHUR}} / (1 - \gamma + \gamma D^{\text{Fe}}). \quad (\text{A5})$$

Although the expressions for these concentrations correspond to equilibrium values, it does not mean that the bulk core is in equilibrium with the bulk mantle. Similar equations apply to Ni and the f_m and f_c values also remain constant. We can write the following mass balance equation for Ni and Fe between the mantle, core, and bulk planet assumed to be chondritic,

$$[\text{Ni}]_c M_c + [\text{Ni}]_m M_m = [\text{Ni}]_{\text{CHUR}} (M_m + M_c), \quad (\text{A6})$$

$$(\text{Fe}/\text{Ni})_c [\text{Ni}]_c M_c + (\text{Fe}/\text{Ni})_m [\text{Ni}]_m M_m = (\text{Fe}/\text{Ni})_{\text{CHUR}} [\text{Ni}]_{\text{CHUR}} (M_m + M_c). \quad (\text{A7})$$

If we form the difference (A7)-(A6) and divide by $(\text{Fe}/\text{Ni})_{\text{CHUR}}$, we obtain the relationship,

$$f_c [\text{Ni}]_c M_c + f_m [\text{Ni}]_m M_m = 0. \quad (\text{A8})$$

We therefore have,

$$\frac{[\text{Ni}]_c M_c}{[\text{Ni}]_m M_m} = -\frac{f_m}{f_c}, \quad (\text{A9})$$

and similarly,

$$\frac{[\text{Ni}]_c M_c + [\text{Ni}]_m M_m}{[\text{Ni}]_m M_m} = \frac{[\text{Ni}]_{\text{CHUR}} M}{[\text{Ni}]_m M_m} = 1 - \frac{f_m}{f_c}. \quad (\text{A10})$$

We can now write a differential equation for ^{60}Ni in the mantle,

$$\begin{array}{l} \text{change in the mantle} \\ d(M_m [^{58}\text{Ni}]_m R_m) \end{array} = \begin{array}{l} \text{extraterrestrial delivery} \\ [^{58}\text{Ni}]_{\text{CHUR}} R_{\text{CHUR}} d(M_m + M_c) \end{array} - \begin{array}{l} \text{removal to the core} \\ [^{58}\text{Ni}]_c R_m dM_c \end{array} + \begin{array}{l} \text{radioactive decay} \\ \lambda M_m [^{60}\text{Fe}]_m dt \end{array}. \quad (\text{A11})$$

Here it is assumed that the impactor is well-mixed and homogenized in the mantle, so that each increment of metal that is removed to the core has the isotopic composition of the mantle. We have just seen that the concentration in the mantle remains constant, so $[^{58}\text{Ni}]_m$ in the left term can be taken out of the differential,

$$[^{58}\text{Ni}]_m d(M_m R_m) = [^{58}\text{Ni}]_{\text{CHUR}} R_{\text{CHUR}} dM - [^{58}\text{Ni}]_c R_m dM_c + \lambda M_m [^{60}\text{Fe}]_m dt, \quad (\text{A12})$$

$$[^{58}\text{Ni}]_m R_m dM_m + [^{58}\text{Ni}]_m M_m dR_m = [^{58}\text{Ni}]_{\text{CHUR}} R_{\text{CHUR}} dM - [^{58}\text{Ni}]_c R_m dM_c + \lambda M_m [^{60}\text{Fe}]_m dt. \quad (\text{A13})$$

All the terms can be divided by $[^{58}\text{Ni}]_m M_m$ to yield,

$$R_m d\ln M_m + dR_m = \frac{[^{58}\text{Ni}]_{\text{CHUR}} M}{[^{58}\text{Ni}]_m M_m} R_{\text{CHUR}} d\ln(M) - \frac{[^{58}\text{Ni}]_c M_c}{[^{58}\text{Ni}]_m M_m} R_m d\ln(M_c) + \lambda \left(\frac{^{60}\text{Fe}}{^{58}\text{Ni}} \right)_m dt. \quad (\text{A14})$$

Because we assume $\gamma = \text{constant}$, we have $d\ln(M_c) = d\ln(M_m) = d\ln(M)$. Injecting Eqs. A9 and A10 into Eq. A14, it follows,

$$dR_m = -R_m d\ln(M) + \left(1 - \frac{f_m}{f_c}\right) R_{\text{CHUR}} d\ln(M) + \frac{f_m}{f_c} R_m d\ln(M) + \lambda \left(\frac{^{60}\text{Fe}}{^{58}\text{Ni}} \right)_m dt, \quad (\text{A15})$$

$$dR_m = \left(\frac{f_m}{f_c} - 1 \right) (R_m - R_{\text{CHUR}}) d\ln(M) + \lambda (f_m + 1) \left(\frac{^{60}\text{Fe}}{^{58}\text{Ni}} \right)_{\text{CHUR}} dt. \quad (\text{A16})$$

The differential equation governing the change in Ni isotopic composition of the CHUR reservoir is,

$$dR_{\text{CHUR}} = \lambda \left(\frac{^{60}\text{Fe}}{^{58}\text{Ni}} \right)_{\text{CHUR}} dt. \quad (\text{A17})$$

Eq. A16 can therefore be rewritten as,

$$d(R_m - R_{\text{CHUR}}) = \left(\frac{f_m}{f_c} - 1\right) (R_m - R_{\text{CHUR}}) d\ln(M) + \lambda f_m \left(\frac{{}^{60}\text{Fe}}{{}^{58}\text{Ni}}\right)_{\text{CHUR}} dt. \quad (\text{A18})$$

If we pose $X = R_m - R_{\text{CHUR}}$ and express the $({}^{60}\text{Fe}/{}^{58}\text{Ni})_{\text{CHUR}}$ ratio as a function of the ratio at the time of CAI formation, we have,

$$dX = \left(\frac{f_m}{f_c} - 1\right) X d\ln(M) + \lambda f_m \left(\frac{{}^{60}\text{Fe}}{{}^{58}\text{Ni}}\right)_{\text{CHUR},0} e^{-\lambda t} dt. \quad (\text{A19})$$

This equation can be solved analytically using the initial condition $X(t = 0) = 0$,

$$R_m(t) - R_{\text{CHUR}}(t) = \lambda f_m \left(\frac{{}^{60}\text{Fe}}{{}^{58}\text{Ni}}\right)_{\text{CHUR},0} \int_0^t \left[\frac{M(x)}{M(t)}\right]^{1-\frac{f_m}{f_c}} e^{-\lambda x} dx. \quad (\text{A20})$$

In ϵ notation, this takes the form,

$$\epsilon^{60}\text{Ni}_m(t) - \epsilon^{60}\text{Ni}_{\text{CHUR}}(t) = \lambda f_m 10^4 \left(\frac{{}^{56}\text{Fe}}{{}^{60}\text{Ni}}\right)_{\text{CHUR}} \left(\frac{{}^{60}\text{Fe}}{{}^{56}\text{Fe}}\right)_{\text{CHUR},0} \int_0^t \left[\frac{M(x)}{M(t)}\right]^{1-\frac{f_m}{f_c}} e^{-\lambda x} dx. \quad (\text{A21})$$

If we introduce $q_{\text{Ni}} = 10^4 \left(\frac{{}^{56}\text{Fe}}{{}^{60}\text{Ni}}\right)_{\text{CHUR}}$, we have,

$$\epsilon^{60}\text{Ni}_m(t) - \epsilon^{60}\text{Ni}_{\text{CHUR}}(t) = \lambda f_m q_{\text{Ni}} \left(\frac{{}^{60}\text{Fe}}{{}^{56}\text{Fe}}\right)_{\text{CHUR},0} \int_0^t \left[\frac{M(x)}{M(t)}\right]^{1-\frac{f_m}{f_c}} e^{-\lambda x} dx. \quad (\text{A22})$$

No core sample is usually available to measure f_c but this quantity can be estimated by combining estimates of the mantle and CHUR (bulk planet) compositions (Eq. A10),

$$f_c = \frac{[\text{Ni}]_m M_m}{[\text{Ni}]_m M_m - [\text{Ni}]_{\text{CHUR}} M} f_m. \quad (\text{A23})$$

Appendix B. Supplementary materials

Supplementary data associated with this article can be found in the online version at ...

Reference:

- Asphaug E., Jutzi M. Movshovitz, N., 2011. Chondrule formation during planetesimal accretion. *Earth Planet. Sci. Lett.* **308**, 369-379.
- Boley A.C., Morris M.A., Desch S.J. (2013) High-temperature processing of solids through solar nebular bow shocks: 3D radiation hydrodynamics simulations with particles. *Astrophysical Journal*, in press.
- Boss A. P., Durisen, R. H., 2005. Chondrule-forming shock fronts in the solar nebula: A possible unified scenario for planet and chondrite formation. *Astrophys. J.* **621**, L137-L140.
- Burkhardt C., Kleine T., Oberli F., Pack A., Bourdon B., Wieler R., 2011. Molybdenum isotope anomalies in meteorites: Constraints on solar nebula evolution and origin of the Earth. *Earth. Planet. Sci. Lett.* **312**, 390-400.
- Burkhardt C., Kleine T., Dauphas N., Wieler R., 2012. Nucleosynthetic tungsten isotope anomalies in acid leachates of the Murchison chondrite: Implications for hafnium-tungsten chronometry. *Astrophys. J.* **753**, L6-L11.
- Cameron A. G., Ward W. R., 1976. The origin of the Moon. *Lunar Planet. Sci. Conf.* **7**, 120.
- Canup R. M., Asphaug E., 2001. Origin of the Moon in a giant impact near the end of the Earth's formation. *Nature* **412**, 708-712.
- Canup R. M., 2012. Forming a Moon with an Earth-like Composition via a Giant Impact. *Science* **338**, 1052-1055.
- Caro G., Bourdon B., Halliday A.N., Quitté G., 2008. Super-chondritic Sm/Nd ratios in Mars, the Earth and the Moon. *Nature* **452**, 336-339.

- Chambers J.E., Wetherill G.W., 1998. Making the terrestrial planets: N-body integrations of planetary embryos in three dimensions. *Icarus* **136**, 304-327.
- Chambers J. E., 2004. Planetary accretion in the inner Solar System. *Earth Planet. Sci. Lett.* **223**, 241-252.
- Chambers J. E., 2006. Planet formation with migration. *Astrophys. J.* **652**, L133-L136.
- Chen J.H., Papanastassiou D.A., Telus M., Huss G.R., 2013. Fe-Ni isotopic systematics in UOC Que 97008 and Semarkona Chondrules. *Lunar Planet. Sci. Conf. XLIV* #2649.
- Clayton R. N., Mayeda T. K., 1983. Oxygen isotopes in eucrites, shergottites, nakhlites, and chassignites. *Earth Planet. Sci. Lett.* **62**, 1-6.
- Clayton R.N., Mayeda T.K., Rubin A.E., 1984. Oxygen isotope compositions of enstatite chondrites and aubrites. *J. Geophys. Res.* **89**, C245-C249.
- Clayton R.N., Mayeda T.K., Goswami J.N., Olsen E.J., 1991. Oxygen isotope studies of ordinary chondrites. *Geochim. Cosmochim. Acta* **35**, 2317-2338.
- Clayton R.N., Mayeda T.K., 1999. Oxygen isotope studies of carbonaceous chondrites. *Geochim. Cosmochim. Acta* **63**, 2089-2104.
- Ćuk M., Stewart S. T., 2012. Making the Moon from a fast-spinning Earth: A giant impact followed by resonant despinning. *Science* **338**, 1047-1052.
- Dahl T. W., Stevenson D. J., 2010. Turbulent mixing of metal and silicate during planet accretion—And interpretation of the Hf–W chronometer. *Earth Planet. Sci. Lett.* **295**, 177-186.

- Dauphas N., Chaussidon M., 2011. A perspective from extinct radionuclides on a young stellar object: The sun and its accretion disk. *Annu. Rev. Earth Planet. Sci.* **39**, 351-386.
- Dauphas N., Pourmand A., 2011. Hf-W-Th evidence for rapid growth of Mars and its status as a planetary embryo. *Nature* **473**, 489-492.
- Dauphas N., Marty B., Reisberg, L., 2002a. Molybdenum nucleosynthetic dichotomy revealed in primitive meteorites. *Astrophys. J.* **569**, L139-L142.
- Dauphas N., Marty B., Reisberg L., 2002b. Inference on terrestrial genesis from molybdenum isotope systematics. *Geophys. Res. Lett.* **29**, 1084.
- Dauphas N., Cook D.L., Sacarabany A., Fröhlich C., Davis A.M., Wadhwa M., Pourmand A, Rauscher T., Gallino R., 2008. Iron-60 evidence for early injection and efficient mixing of stellar debris in the protosolar nebula. *Astrophys. J.* **686**, 560-569.
- Dauphas N., Remusat L., Chen J.H., Roskosz M., Papanastassiou D.A., Stodolna J., Guan Y., Ma C., Eiler J.M. 2010. Neutron-rich chromium isotope anomalies in supernova nanoparticles. *Astrophys. J.* **720**, 1577-1591.
- Debaille V., Brandon A.D., Yin Q.Z., Jacobsen S.B., 2007. Coupled ^{142}Nd - ^{143}Nd evidence for a protracted magma ocean in Mars. *Nature* **450**, 525-528.
- Deguen R., Olson P., Cardin P., 2011. Experiments on turbulent metal-silicate mixing in a magma ocean. *Earth Planet. Sci. Lett.* **310**, 303-313.
- Fedkin A. V., Grossman L., 2013. Vapor saturation of sodium: Key to unlocking the origin of chondrules. *Geochim. Cosmochim. Acta* **112**, 226-250.
- Foley C.N., Wadhwa M., Borg L.E., Janney P.E., Hines R., Grove T.L., 2005. The early

differentiation history of Mars from ^{182}W - ^{142}Nd isotope systematics in SNC meteorites. *Geochim. Cosmochim. Acta.* **69**, 4557-4571.

Gramlich J.W., Machlan L.A., Barnes I.L., Paulsen P.J., 1989. Absolute isotopic abundance ratios and atomic weight of a reference sample of nickel. *J. Res. N.I.S.T.* **94**, 347-356.

Grimm R.E., McSween H.Y.Jr., 1993. Heliocentric zoning of the asteroid belt by aluminum-26 heating. *Science* **259**, 653-655.

Guan Y., Huss G. R., Leshin L. A., 2007. ^{60}Fe - ^{60}Ni and ^{53}Mn - ^{53}Cr isotopic systems in sulfides from unequilibrated enstatite chondrites. *Geochim. Cosmochim. Acta* **71**, 4082-4091.

Halliday A.N., Rehkämper M., Lee D.C., Yi W., 1996. Early evolution of the Earth and Moon: New constraints from Hf-W isotope geochemistry. *Earth Planet. Sci. Lett.* **142**, 75-89.

Halliday, A.N. 2004. Mixing, volatile loss and compositional change during impact - driven accretion of the Earth. *Nature* **427**, 505-509.

Harper C.L., Nyquist L., Wiesmann H., Shih C.-Y., 1995. Rapid accretion and early differentiation of Mars indicated by ^{142}Nd - ^{144}Nd in SNC meteorites. *Science* **267**, 213-217.

Harper C.L., Jacobsen S.B., 1996. Evidence for ^{182}Hf in the early solar system and constraints on the timescale of terrestrial accretion and core formation. *Geochim. Cosmochim. Acta.* **60**, 1131-1153.

Harris D.C., 2011. Quantitative Chemical Analysis, Eighth Edition. W.H. Freeman, pp. 750.

- Hartmann W. K., Davis D. R. 1975. Satellite-sized planetesimals and lunar origin. *Icarus* **24**, 504-515.
- Horwitz E.P., Dietz M.L., Chiarizia R., Diamond H. 1992. Separation and preconcentration of uranium from acidic media by extraction chromatography. *Anal. Chim. Acta* **266**, 25-37.
- Ito E., Katsura T., Suzuki T., 1998. Metal/Silicate partitioning of Mn, Co, and Ni at high pressures and high temperatures and implications for core formation in a deep magma ocean. In *Properties of Earth and Planetary Materials at High Pressure and Temperature* (eds. M. H. Manghnani and T. Yagi) Geophysical Monograph, 101 (1998), pp. 215–225.
- Jacobsen S.B., 2005. The Hf-W isotopic system and the origin of the Earth and Moon. *Annu. Rev. Earth Planet. Sci.* **33**, 531-570.
- Jagoutz E., Dreibus G., Jotter R., 2003. New ¹⁴²Nd data on SNC meteorites. *Geochim. Cosmochim. Acta.* **67**, A184.
- Kita N.T. , Huss G.R. , Tachibana S., Amelin Y., Nyquist L.E., Hutcheon I.D., 2005. Constraints on the origin of chondrules and CAIs from short-lived and long-lived radionuclides. In *Chondrites and the Protoplanetary Disk. ASP conf. Ser.* **341** (San Francisco: ASP), 558-587.
- Kleine T., Münker C., Mezger K., Palme H., 2002. Rapid accretion and early core formation on asteroids and the terrestrial planets from Hf-W chronometry. *Nature* **418**, 952-955.

- Kleine T., Touboul M., Bourdon B., Nimmo F., Mezger K., Palme H., Jacobsen S.B., Yin Q.-Z., Halliday A.N. 2009. Hf-W chronology of the accretion and early evolution of asteroids and terrestrial planets. *Geochim. Cosmochim. Acta* **73**, 5150-5188.
- Kleine T., Mezger K., Münker C., Palme H., Bischoff A., 2004a. ^{182}Hf - ^{182}W isotope systematics of chondrites, eucrites, and martian meteorites: Chronology of core formation and early mantle differentiation in Vesta and Mars. *Geochim. Cosmochim. Acta*. **68**, 2935-2946.
- Kleine T., Mezger K., Palme H., Münker C., 2004b. The W isotope evolution of the bulk silicate Earth: constraints on the timing and mechanisms of core formation and accretion. *Earth Planet. Sci. Lett.* **228**, 109-123.
- Kleine T., Mezger K., Palme H., Scherer E., Münker C., 2005. Early core formation in asteroids and late accretion of chondrite parent bodies: Evidence from ^{182}Hf - ^{182}W in CAIs, metal-rich chondrites, and iron meteorites. *Geochim. Cosmochim. Acta* **69**, 5805-5818.
- Kobayashi H., Dauphas N., 2013. Small planetesimals in a massive disk formed Mars. *Icarus* **225**, 122-130.
- Kruijer T.S., Fischer-Gödde. M., Kleine T., Sprung P., Leya I., Wieler R., 2012. Neutron capture on Pt isotopes in iron meteorites and the Hf-W chronology of core formation in planetesimals. *Earth Planet. Sci. Lett.* **361**, 162-172.
- Lapen T.J., Righter M., Brandon A.D., Debaille V., Beard B.L., Shafer J.T., Peslier A.H. , 2010. A younger age for ALH84001 and its geochemical link to Shergottite sources in Mars. *Science* **328**, 347-351.
- Lee D.C., Halliday A.N., 1997. Core formation on Mars and differentiated asteroids.

Nature **388**, 854-857.

Li J., Agee C. B., 1996. Pressure effect on partitioning of Ni, Co, S: implications for mantle-core formation. *Lunar Planet. Sci.* **27**, 749.

Maréchal C.N., Tédouk P. and Albarède F., 1999. Precise analysis of copper and zinc isotopic compositions by plasma-source mass spectrometry. *Chem. Geol.* **156**, 251-272.

Marhas K. K. and Mishra R. K., 2012. Fossil recode of ^{60}Fe in QUE 97008 Chondrule. *75th MetSoc* #5273.

Markowski, A., Quitté G., Halliday, A. N., Kleine, T., 2006. Tungsten isotopic compositions of iron meteorites: chronological constraints vs. cosmogenic effects. *Earth Planet. Sci. Lett.* **242**, 1-15.

Mishra R. K., Goswami J. N., Tachibana S., Huss G. R., Rudraswami N. G., 2010. ^{60}Fe and ^{26}Al in chondrules from unequilibrated chondrites: Implication for early solar system processes. *Astrophys. J.* **714**, L217-L221.

Mishra R. K. and Chaussidon M., 2012. ^{60}Fe - ^{60}Ni isotope systematics in silicates in chondrules from unequilibrated chondrites: Yet again and status Quo. *75th MetSoc* #5194.

Morishima R., Golabek, G. J., Samuel H., 2013. *N*-body simulations of oligarchic growth of Mars: Implications for Hf–W chronology. *Earth Planet. Sci. Lett.* **366**, 6-16.

Morris M. A., Boley A. C., Desch S. J., Athanassiadou T., 2012. Chondrule formation in bow shocks around eccentric planetary embryos. *Astrophys. J.* **752**, 27.

Mostefaoui S., Lugmair G. W., Hoppe P., 2005. ^{60}Fe : a heat source for planetary differentiation from a nearby supernova explosion. *Astrophys. J.* **625**, 271-277.

- Mostefaoui S., Lugmair G.W., Hoppe P., El Goresy A. 2004. Evidence for live ^{60}Fe in meteorites. *New. Astro. Rev.* **48**, 155-159.
- Moynier F., Albarède F., Herzog G.F., 2006. Isotopic composition of zinc, copper, and iron in lunar samples. *Geochim. Cosmochim. Acta.* **70**, 6103-6117.
- Nimmo F., Agnor C.B., 2006. Isotopic outcomes of N-body accretion simulations: Constraints on equilibration processes during large impacts from Hf/W observation. *Earth Planet. Sci. Lett.* **243**, 26-43.
- Nimmo F., O'Brien D. P., Kleine T., 2010. Tungsten isotopic evolution during late-stage accretion: Constraints on Earth–Moon equilibration. *Earth Planet. Sci. Lett.* **292**, 363-370.
- Pierens A., Raymond S. N., 2011. Two phase, inward-then-outward migration of Jupiter and Saturn in the gaseous solar nebula. *Astro. & Astrophys.* **533**, A131.
- Qin L., Dauphas N., Wadhwa M., Markowski A., Gallino R., Janney P.E., Bouman C. 2008. Tungsten nuclear anomalies in planetesimal cores. *Astrophys. J.* **674**, 1234-1241.
- Qin L., Alexander C.M.D., Carlson R.W., Horan M.F., Yokoyama T., 2010. Contributors to chromium isotope variation of meteorites. *Geochim. Cosmochim. Acta* **74**, 1122-1145.
- Qin L., Nittler L. R., Alexander C. M., Wang J., Stadermann F. J., Carlson R. W., 2011. Extreme ^{54}Cr -rich nano-oxides in the CI chondrite Orgueil—Implication for a late supernova injection into the solar system. *Geochim. Cosmochim. Acta* **75**, 629-644.

- Quitté G., Markowski A., Latkoczy C., Gabriel A., Pack A., 2010. Iron-60 heterogeneity and incomplete isotope mixing in the early solar system. *Astrophys. J.* **720**, 1215-1224.
- Quitté G., Latkoczy C., Schönbacher M., Halliday A.N., Günther D., 2011. ^{60}Fe - ^{60}Ni systematics in the eucrite parent body: A case study of Bouvante and Juvinas. *Geochim. Cosmochim. Acta* **75**, 7698-7706.
- Raymond S.N., O'Brien D.P., Morbidelli A., Kaib A., 2009. Building the terrestrial planets: constrained accretion in the inner solar system. *Icarus* **203**, 644-662.
- Regelous M., Elliott T., Coath C.D., 2008. Nickel isotope heterogeneity in the early Solar System. *Earth Planet. Sci. Lett.* **272**, 330-338.
- Reufer A., Meier M. M., Benz W., Wieler R., 2012. A hit-and-run giant impact scenario. *Icarus* **221**, 296-299.
- Rubie D. C., Melosh H. J., Reid J. E., Liebske C., Righter K., 2003. Mechanisms of metal-silicate equilibration in the terrestrial magma ocean. *Earth Planet. Sci. Lett.* **205**, 239-255.
- Rudge J. F., Kleine T., Bourdon B., 2010. Broad bounds on Earth's accretion and core formation constrained by geochemical models. *Nature Geo.* **3**, 439-443.
- Rugel G., Faestermann T., Knie K., Korschinek G., Poutivtsev M., Schumann D., Kivel N., Gunther-Leopold I., Weinreich R., Wohlmuther M., 2009. New measurement of the ^{60}Fe half-life. *Phys. Rev. Lett.* **103**, 072502.
- Samuel H., 2012. A re-evaluation of metal diapir breakup and equilibration in terrestrial magma oceans. *Earth Planet. Sci. Lett.* **313**, 105-114.

- Sanders I. S., Scott E. R., 2012. The origin of chondrules and chondrites: Debris from low-velocity impacts between molten planetesimals? *Meteo. Planet. Sci.* **47**, 2170-2192.
- Sanloup C., Jambon A., Gillet P., 1999. A simple chondritic model of Mars. *Phys. Earth Planet. Inter.* **112**, 43-54.
- Scherstén A., Elliott T., Hawkesworth C., Russell S., Masarik J., 2006. Hf–W evidence for rapid differentiation of iron meteorite parent bodies. *Earth Planet. Sci. Lett.* **241**, 530-542.
- Spivak-Birndorf L. J., Wadhwa M., Janney P. E., 2012. ^{60}Fe – ^{60}Ni systematics of Chainpur chondrules and the plutonic angrites Northwest Africa 4590 and 4801. *Lunar Planet. Sci.* **XLIII**, #2861.
- Steele R.C.J., Elliott T., Coath C. D., Regelous M., 2011. Confirmation of mass-independent Ni isotopic variability in iron meteorites. *Geochim. Cosmochim. Acta* **75**, 7906-7925.
- Steele R.C.J., Coath C.D., Regelous M., Russell S., Elliott T., 2012. Neutron-poor nickel isotope anomalies in meteorites. *Astrophys. J.* **758**, 59-80.
- Strelow F.W.E., Victor A.H., van Zyl C.R., Eloff C., 1971. Distribution coefficients and cation exchange behavior of elements in hydrochloric acid-acetone. *Anal. Chem.* **43**, 870-876.
- Sugiura N., Miyazaki A., Yin Q.-Z., 2006. Heterogeneous distribution of ^{60}Fe in the early solar nebula: achondrite evidence. *Earth Planets Space* **58**, 1079-1086.
- Tachibana S., Huss G. R., 2003. The initial abundance of Fe-60 in the solar system. *Astrophys. J.* **588**, L41-L44.

- Tachibana S., Huss G.R., Kita N.T., Shimoda G., Morishita Y., 2006. ^{60}Fe in chondrites: Debris from a nearby supernova in the early Solar System? *Astrophys. J.* **639**, L87-L90.
- Tang H., Dauphas N., 2012. Abundance, distribution, and origin of ^{60}Fe in the solar protoplanetary disk. *Earth. Planet. Sci. Lett.* **359-360**, 248-263.
- Thibault Y., Walter M. J., 1995. The influence of pressure and temperature on the metal-silicate partition coefficients of nickel and cobalt in a model C1 chondrite and implications for metal segregation in a deep magma ocean. *Geochim. Cosmochim. Acta* **59**, 991-1002.
- Thommes E. W., Duncan M. J., Levison H. F., 2001. Solar System Formation Time Scales From Oligarchic Growth. In *Astrophysical Ages and Times Scales. ASP conf. Ser.* (eds von Hoppel, T., Simpson, C., Manset, N.) **245**, 91-100.
- Touboul M., Puchtel I.S., Walker R.J., 2012. ^{182}W evidence for long-term preservation of early mantle differentiation products. *Science* **335**, 1065-1069.
- Trinquier A., Birck J.-L., Allegre C.J., 2007. Widespread ^{54}Cr heterogeneity in the inner solar system. *Astrophys. J.* **655**, 1179-1185.
- Trinquier A., Elliott T., Ulfbeck D., Coath C., Krot A.N., Bizzarro M., 2009. Origin of nucleosynthetic heterogeneity in the solar protoplanetary disk. *Science* **324**, 374-376.
- Villeneuve J., Chaussidon M., Libourel G., 2009. Homogeneous distribution of ^{26}Al in the solar system from the Mg isotopic composition of chondrules. *Science* **325**, 985-988.

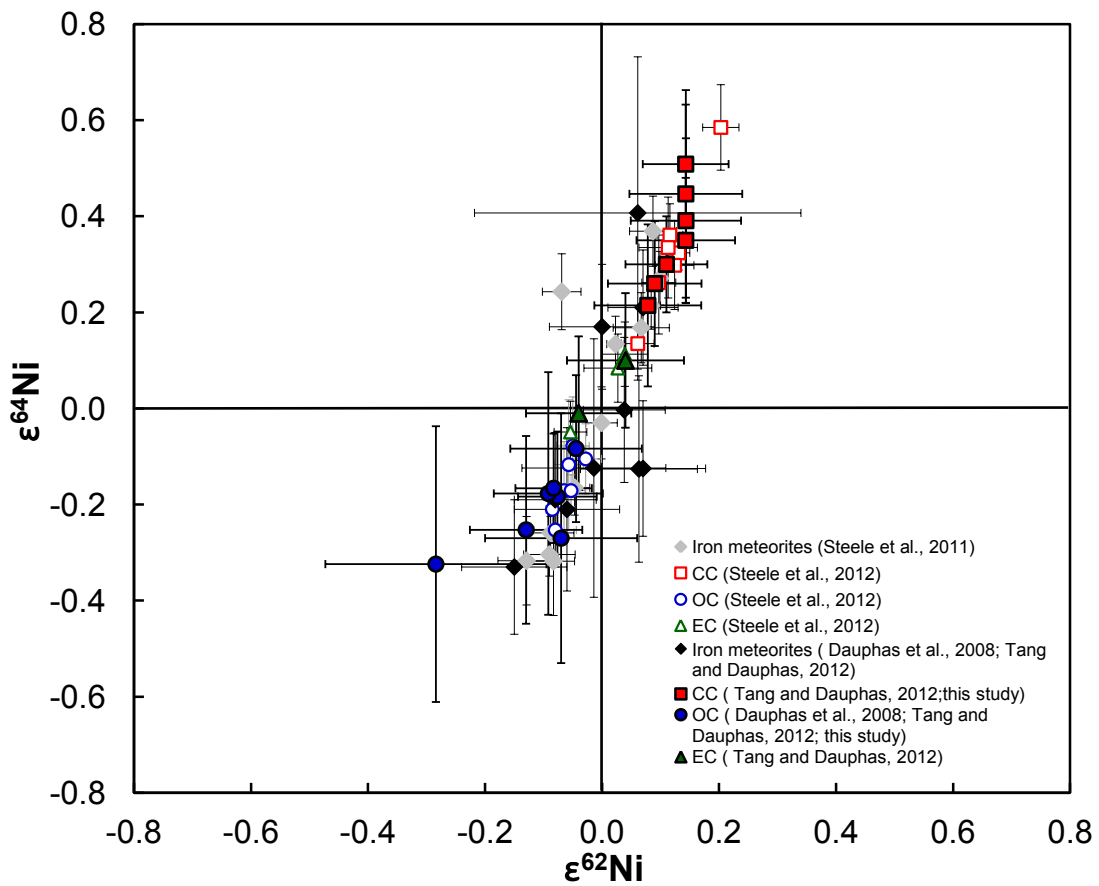
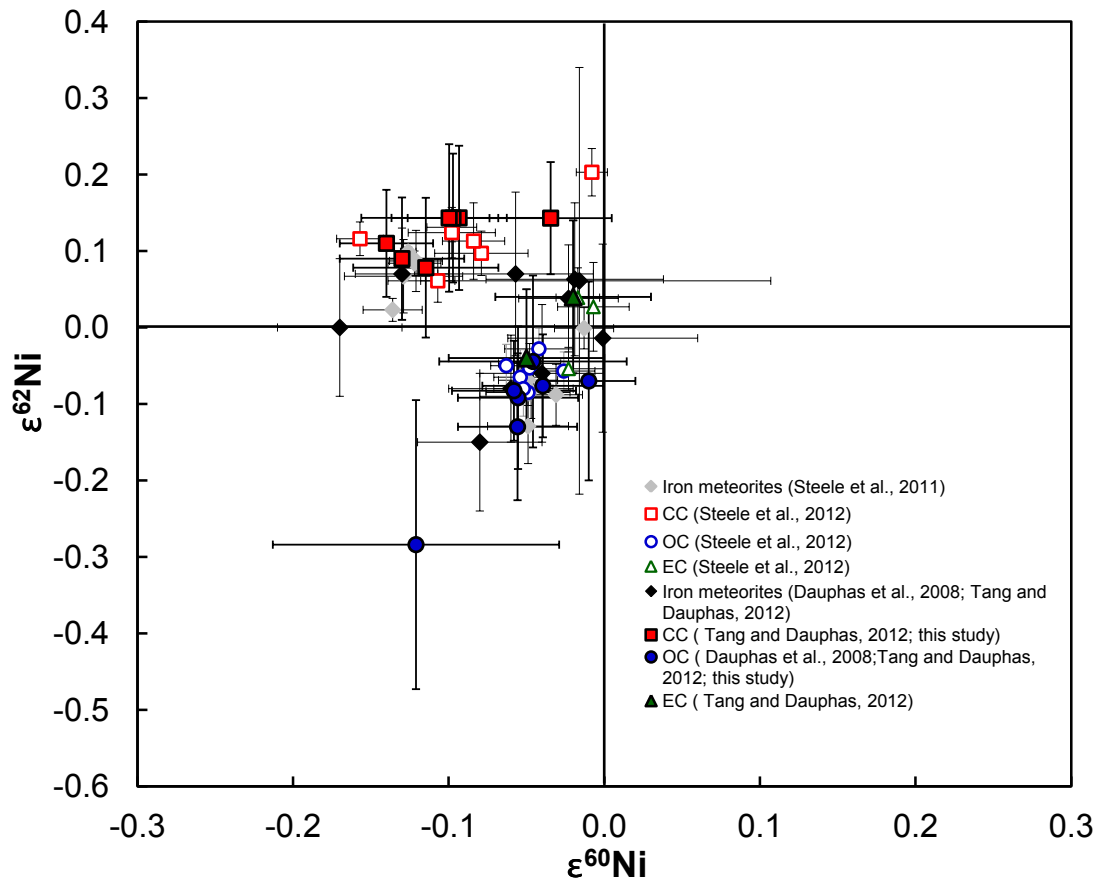
- Wadhwa M., Srinivasan G., Carlson R. W., 2006. Timescales of planetesimal differentiation in the early solar system. *Meteorites and the Early Solar System II*, Lauretta D.S. and McSween Jr. H. Y. (Eds.), University of Arizona Press, Tucson, **943** pp., p.715-731.
- Walsh K. J., Morbidelli A., Raymond S. N., O'Brien D. P., Mandell, A. M., 2011. A low mass for Mars from Jupiter's early gas-driven migration. *Nature* **475**, 206-209.
- Wänke H., Dreibus, G., 1988. Chemical composition and accretion history of terrestrial planets. *Phil. Trans. R. Soc. Lond. A* **325**, 545-557.
- Warren P. H., Kallemeyn G.W., Kyte F.T., 1999. Origin of planetary cores: Evidence from highly siderophile elements in martian meteorites. *Geochim. Cosmochim. Acta* **63**, 2105-2122.
- Warren P. H., 2011. Stable-isotopic anomalies and the accretionary assemblage of the Earth and Mars: A subordinate role for carbonaceous chondrites. *Earth. Planet. Sci. Lett.* **311**, 93-100.
- Wasson J. T., Kallemeyn G. W., 1988. Compositions of chondrites. *Phil. Trans. R. Soc. Lond. A* **325**, 535-544.
- Weisberg M. K., Prinz M., Clayton R. N., Mayeda T. K., Sugiura N., Zashu S., Ebihara M., 2001. A new metal - rich chondrite grouplet. *Meteo. Planet. Sci.* **36**, 401-418.
- Wetherill G.W., 1991. Why isn't Mars as big as Earth? *Lunar Planet. Sci.* **22**, 1495-1496.
- Willbold M., Elliott T., Moorbath S., 2011. The tungsten isotopic composition of the Earth's mantle before the terminal bombardment. *Nature* **477**, 195-198.

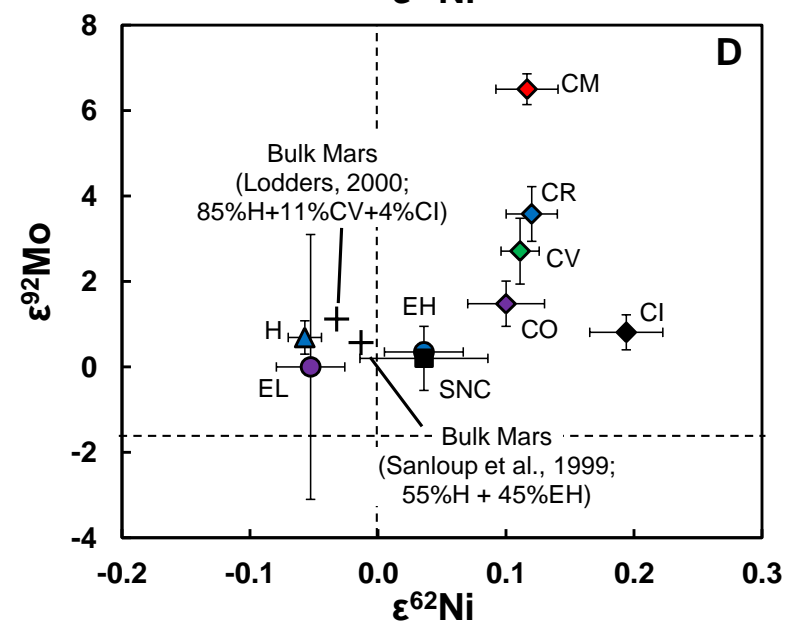
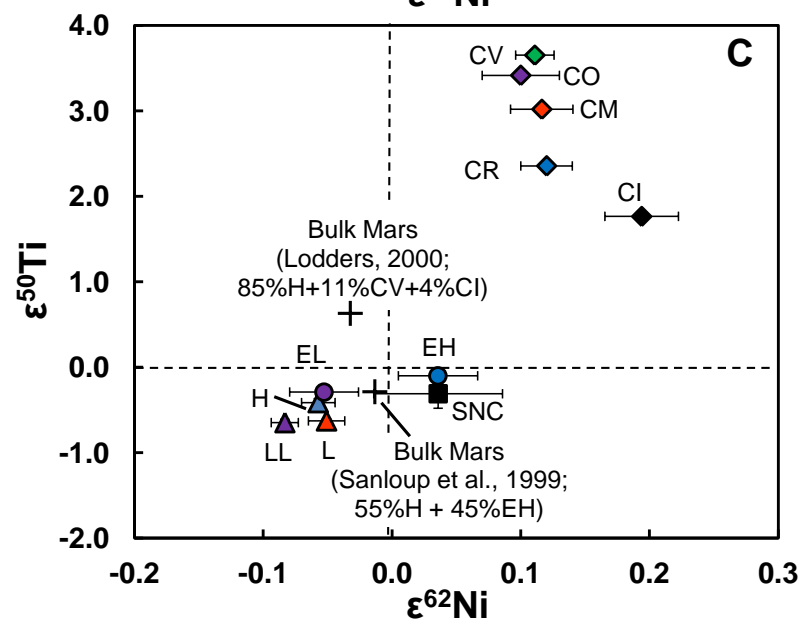
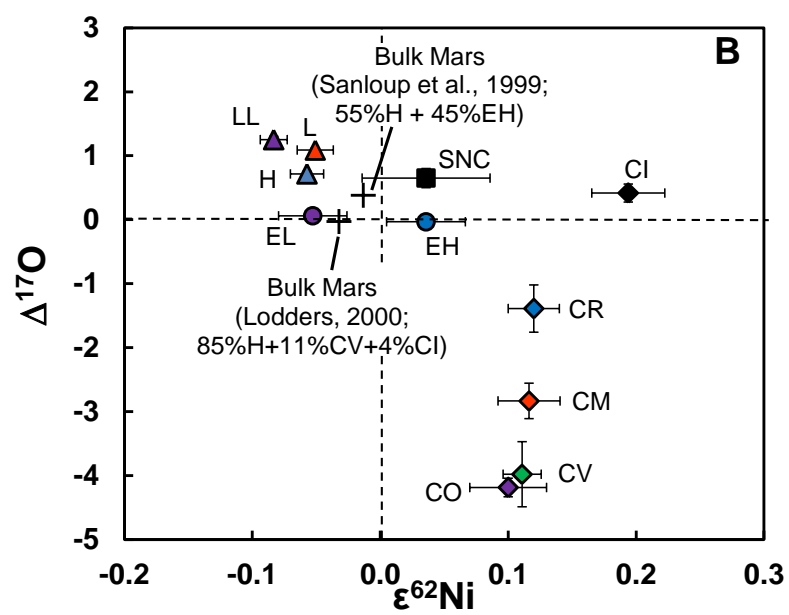
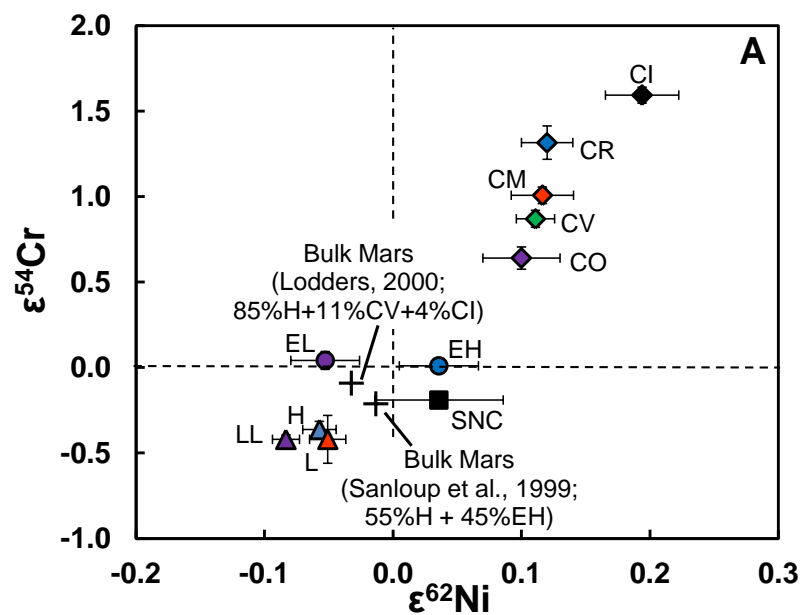
- Wittig N., Humayun M., Brandon A. D., Huang S., Leya I., 2012. Coupled W–Os–Pt isotope systematics in IVB iron meteorites: In situ neutron dosimetry for W isotope chronology. . *Earth. Planet. Sci. Lett.* **361**, 152-161.
- Zhang J., Dauphas N., Davis A. M., Leya I., Fedkin A., 2012. The proto-Earth as a significant source of lunar material. *Nature Geo.* **5**, 251-255.

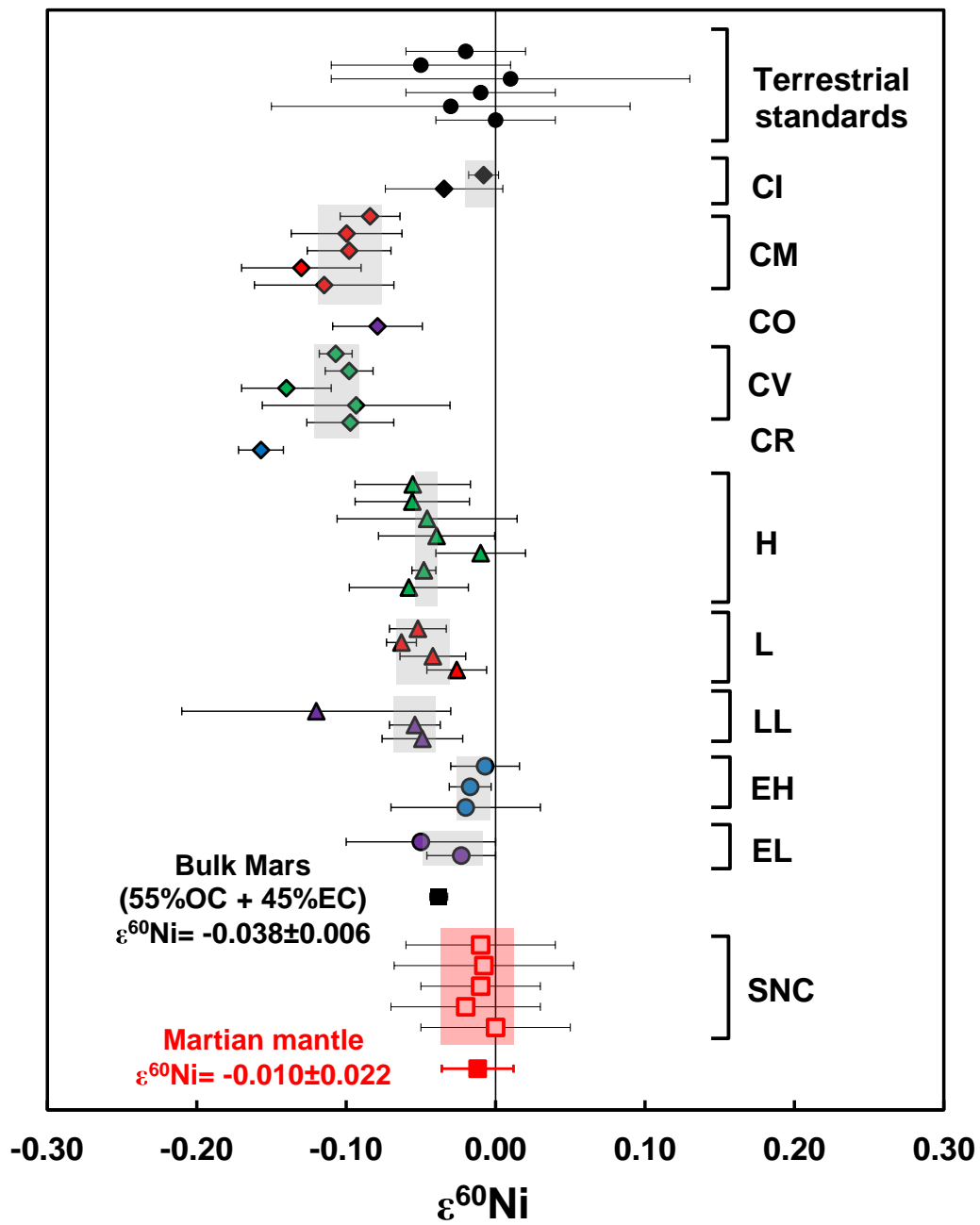
Table 1. Fe/Ni ratios and Ni isotope data of geostandards, chondrites, and martian meteorites.

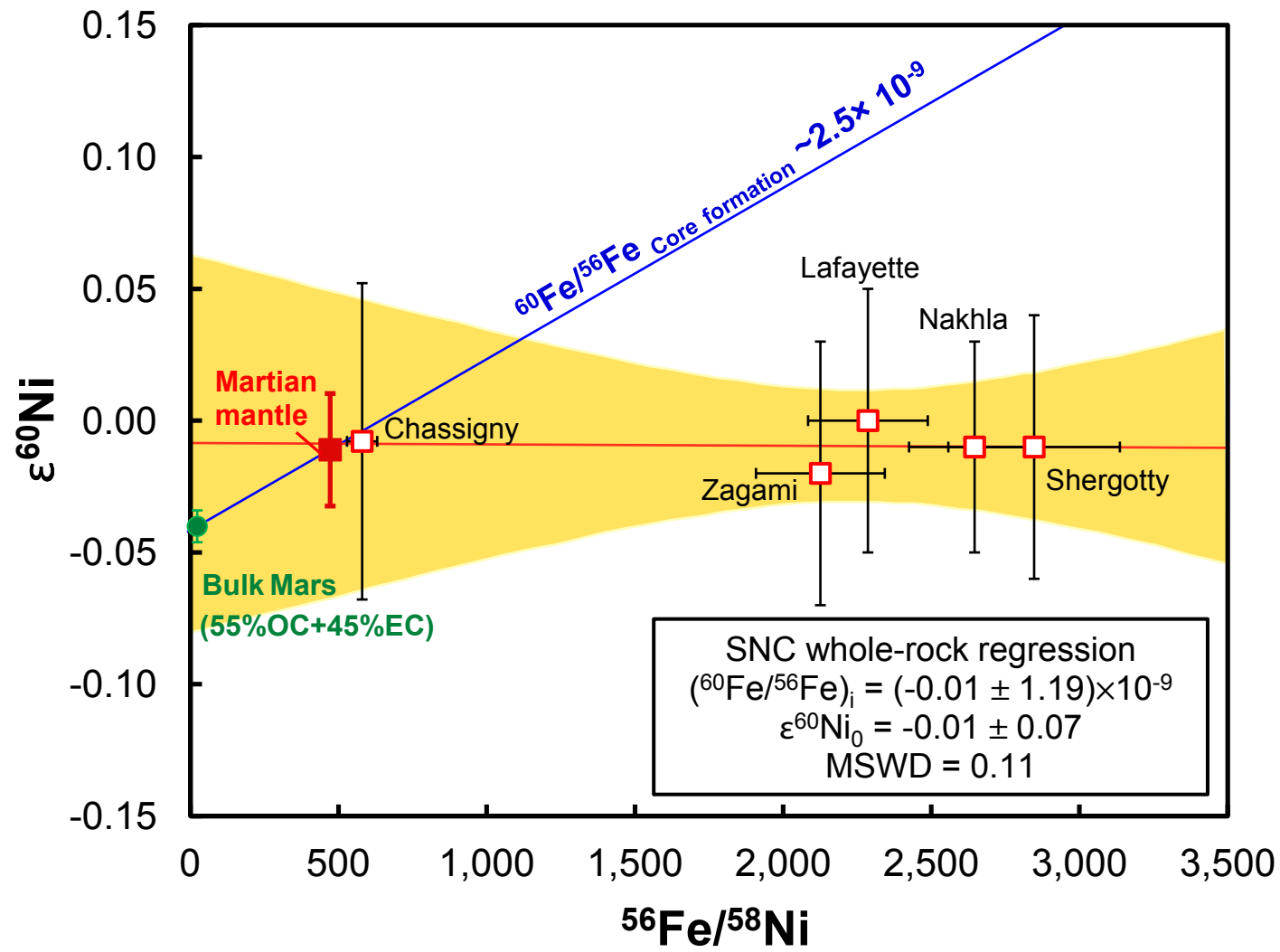
Name	Type	Mass (mg)	Fe/Ni (wt.)	⁵⁶ Fe/ ⁵⁸ Ni (at.)	Norm. ⁶¹ Ni/ ⁵⁸ Ni			Norm. ⁶² Ni/ ⁵⁸ Ni		
					$\epsilon^{60}\text{Ni}$	$\epsilon^{62}\text{Ni}$	$\epsilon^{64}\text{Ni}$	$\epsilon^{60}\text{Ni}$	$\epsilon^{61}\text{Ni}$	$\epsilon^{64}\text{Ni}$
Terrestrial standards										
BE-N		150	342	477 ± 52	-0.02 ± 0.04	0.02 ± 0.09		-0.03 ± 0.04	-0.02 ± 0.06	
BHVO-02		164	710	991 ± 80	-0.05 ± 0.06	-0.11 ± 0.17		0.00 ± 0.05	0.08 ± 0.13	
BHVO-02 (2)		195	727	1010 ± 30	0.01 ± 0.12	-0.04 ± 0.09		-0.01 ± 0.10	0.03 ± 0.04	
DNC-1		187	296	413 ± 33	-0.01 ± 0.05	0.03 ± 0.08		-0.03 ± 0.05	-0.02 ± 0.06	
DNC-1 (2)		105	258	359 ± 23	-0.03 ± 0.12	0.12 ± 0.14		-0.06 ± 0.09	-0.11 ± 0.20	
DTS-02		20	15	21	0.00 ± 0.04	0.01 ± 0.07	-0.05 ± 0.12	0.00 ± 0.03	-0.01 ± 0.05	-0.07 ± 0.10
Weighted Average					-0.02 ± 0.03	0.01 ± 0.04		-0.03 ± 0.03	0.00 ± 0.02	
Mean Square Weighted Deviation (MSWD)					0.28	1.2		0.119	1.19	
Carbonaceous chondrites										
Orgueil	CI	12.8	17	25	-0.03 ± 0.04	0.14 ± 0.07	0.51 ± 0.12	-0.11 ± 0.03	-0.11 ± 0.06	0.06 ± 0.30
Mighei	CM2	10.9	19	26	-0.10 ± 0.04	0.14 ± 0.10	0.55 ± 0.22	-0.17 ± 0.06	-0.11 ± 0.07	0.34 ± 0.14
Murchison	CM2	10.1	19	26	-0.11 ± 0.05	0.08 ± 0.09	0.21 ± 0.17	-0.15 ± 0.03	-0.06 ± 0.07	0.10 ± 0.11
Allende	CV3	11.5	19	26	-0.09 ± 0.06	0.14 ± 0.09	0.39 ± 0.17	-0.17 ± 0.06	-0.11 ± 0.07	0.18 ± 0.10
Vigarano	CV3	14.1	19	26	-0.10 ± 0.03	0.14 ± 0.08	0.35 ± 0.13	-0.17 ± 0.04	-0.11 ± 0.06	0.14 ± 0.10
Weighted Average					-0.09 ± 0.03	0.13 ± 0.04	0.39 ± 0.14	-0.14 ± 0.04	-0.10 ± 0.03	0.17 ± 0.11
MSWD					2.4	0.41	2.2	2.1	0.42	2.1
Ordinary chondrites										
Bath	H4	7.9	15	21	-0.06 ± 0.04	-0.09 ± 0.09	-0.18 ± 0.25	-0.01 ± 0.04	0.07 ± 0.07	-0.04 ± 0.17
Bielokrynitschie	H4	14.1	15	21	-0.06 ± 0.04	-0.13 ± 0.10	-0.25 ± 0.20	0.01 ± 0.04	0.10 ± 0.07	-0.06 ± 0.13
Kesen	H4	10.7	15	21	-0.05 ± 0.06	-0.04 ± 0.11	-0.08 ± 0.15	-0.02 ± 0.03	0.03 ± 0.09	-0.02 ± 0.10
Ochansk	H4	20.3	15	21	-0.04 ± 0.04	-0.08 ± 0.07	-0.18 ± 0.14	0.00 ± 0.04	0.06 ± 0.05	-0.07 ± 0.11
Ste. Marguerite	H4	11.5	15	21	-0.01 ± 0.03	-0.07 ± 0.13	-0.27 ± 0.26	0.03 ± 0.06	0.06 ± 0.10	-0.16 ± 0.18
Kernouvé	H6	31.9	15	21	-0.06 ± 0.04	-0.08 ± 0.07	-0.17 ± 0.11	-0.02 ± 0.03	0.07 ± 0.05	-0.05 ± 0.10
Weighted Average					-0.04 ± 0.02	-0.08 ± 0.03	-0.17 ± 0.06	-0.01 ± 0.02	0.07 ± 0.03	-0.06 ± 0.05
MSWD					1.2	0.31	0.53	0.73	0.34	0.39
Martian meteorites										
Chassigny	Chassignites	111.8	430	600 ± 53	-0.01 ± 0.06	0.04 ± 0.10		-0.03 ± 0.03	-0.03 ± 0.07	
Lafayette	Nakhlites	101.9	1696	2368 ± 210	0.00 ± 0.05	0.05 ± 0.12		-0.03 ± 0.07	-0.04 ± 0.09	
Nakhla	Nakhlites	97.3	1963	2741 ± 230	-0.01 ± 0.04	0.03 ± 0.08		-0.02 ± 0.04	-0.02 ± 0.06	
Shergotty	Shergottites	160.2	2112	2949 ± 301	-0.01 ± 0.05	0.07 ± 0.13		-0.04 ± 0.04	-0.04 ± 0.10	
Zagami	Shergottites	163.2	1577	2202 ± 226	-0.02 ± 0.05	0.01 ± 0.10		-0.03 ± 0.04	-0.01 ± 0.07	
Weighted Average					-0.01 ± 0.02	0.04 ± 0.05		-0.03 ± 0.02	0.03 ± 0.03	
MSWD					0.034	0.16		0.13	0.108	

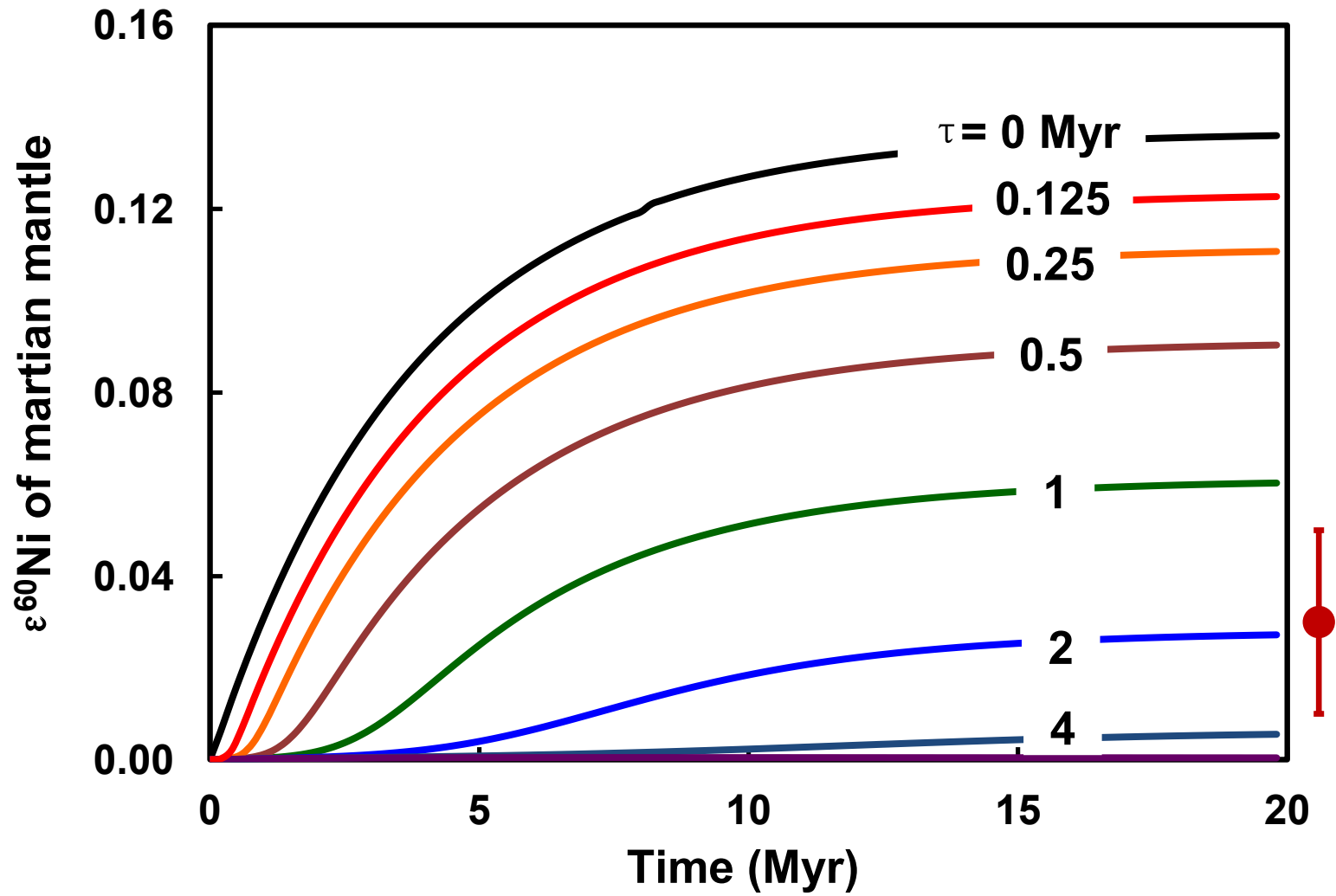
Note: $\epsilon^i\text{Ni} = ([^i\text{Ni}/^{58}\text{Ni}]_{\text{sample}}/[^i\text{Ni}/^{58}\text{Ni}]_{\text{SRM986}} - 1) \times 10^4$. The uncertainties are 95% confidence intervals.











Supporting Online Material to accompany "⁶⁰Fe-⁶⁰Ni Chronology of Core Formation in Mars" by Haolan Tang and Nicolas Dauphas published in Earth and Planetary Science Letters

Table S1. Nickel isotopic compositions in chondrites and Martian meteorites from previous work and this study.

Class	Sample	$\epsilon^{60}\text{Ni}$	95% Conf.	$\epsilon^{62}\text{Ni}$	95% Conf.	Reference
Carbonaceous chondrites						
CI	Orgueil	-0.01	0.01	0.20	0.03	Steele et al., 2012
CI	Orgueil	-0.03	0.04	0.14	0.07	This study
CM2	Cold-Bokkeveld	-0.08	0.02	0.11	0.05	Steele et al., 2012
CM2	Mighei	-0.10	0.04	0.14	0.10	This study
CM2	Murchison	-0.10	0.03	0.12	0.03	Steele et al., 2012
CM2	Murchison	-0.13	0.04	0.09	0.08	Tang et al., 2012
CM2	Murchison	-0.11	0.05	0.08	0.09	This study
CO3	Felix	-0.08	0.03	0.10	0.03	Steele et al., 2012
CV3	Leoville	-0.11	0.01	0.06	0.03	Steele et al., 2012
CV3	Allende	-0.10	0.02	0.13	0.02	Steele et al., 2012
CV3	Allende	-0.14	0.03	0.11	0.07	Tang et al., 2012
CV3	Allende	-0.09	0.06	0.14	0.09	This study
CV3	Vigarano	-0.10	0.03	0.14	0.08	This study
CR2	NWA-801	-0.16	0.02	0.12	0.02	Steele et al., 2012
Weighted average		-0.10	0.02	0.12	0.02	
MSWD		29*		4.1*		
Ordinary chondrites						
H4	Bath	-0.06	0.04	-0.09	0.09	This study
H4	Bielokrynitschie	-0.06	0.04	-0.13	0.10	This study
H4	Kesen	-0.05	0.06	-0.04	0.11	This study
H4	Ochansk	-0.04	0.04	-0.08	0.07	This study
H4	Ste. Marguerite	-0.01	0.03	-0.07	0.13	This study
H6	Butsura	-0.05	0.01	-0.05	0.01	Steele et al., 2012
H6	Kernouvé	-0.06	0.04	-0.08	0.07	This study
H/L3.6	Tieschitz	-0.05	0.02	-0.08	0.04	Steele et al., 2012
L3.7	Ceniceros	-0.06	0.01	-0.05	0.03	Steele et al., 2012
L4	Barratta	-0.04	0.02	-0.03	0.03	Steele et al., 2012
L6	Tenham	-0.03	0.02	-0.06	0.03	Steele et al., 2012
LL3.1	Bishunpur	-0.12	0.09	-0.06	0.10	Dauphas et al., 2008
LL3.4	Chainpur	-0.05	0.02	-0.07	0.04	Steele et al., 2012
LL6	Dhurmsala	-0.05	0.03	-0.09	0.01	Steele et al., 2012
Weighted average		-0.05	0.01	-0.06	0.01	
MSWD		1.8*		2.2*		
Enstatite chondrites						
EH4	Abee	-0.01	0.02	0.03	0.06	Steele et al., 2012
EH5	St.Mark's	-0.02	0.01	0.04	0.04	Steele et al., 2012
EH5	St.Mark's	-0.02	0.05	0.04	0.10	Tang et al., 2012
EL5	Khairpur	-0.05	0.05	-0.04	0.09	Tang et al., 2012
EL6	Khairpur	-0.02	0.02	-0.05	0.03	Steele et al., 2012
Weighted average		-0.02	0.01	0.00	0.04	
MSWD		0.69		4.8*		
Martian chondrites						
	Shergotty	-0.01	0.05	0.07	0.13	This study
	Chassigny	-0.01	0.06	0.04	0.10	This study
	Nakhla	-0.01	0.04	0.03	0.08	This study
	Zagami	-0.02	0.05	0.01	0.10	This study
	Lafayette	0.00	0.05	0.05	0.12	This study
Weighted average		-0.01	0.02	0.04	0.05	
MSWD		0.034		0.16		

* When the MSWD was significantly higher than 1, the weighted average was calculated using Isoplot by weighting the data by a combination of assigned errors and constant external errors to reduce the value of MSWD (Mean Square Weighted) to 1.

Table S2. Compilation of $\Delta^{17}\text{O}$ in chondrites and martian meteorites.

Class	Sample	$\Delta^{17}\text{O}$	Reference	Class	Sample	$\Delta^{17}\text{O}$	Reference	Class	Sample	$\Delta^{17}\text{O}$	Reference
Carbonaceous chondrite											
CI	Alais	0.39	Clayton et al., 1999	CO3	DaG 025	-4.24	Clayton et al., 1999	CK5	EET90004	-4.20	Clayton et al., 1999
CI	Ivuna	0.47	Clayton et al., 1999	CO3	Felix	-4.59	Clayton et al., 1999	CK5	Y 82104	-4.30	Clayton et al., 1999
CI	Orgueil	0.39	Clayton et al., 1999	CO3	HH 043	-4.11	Clayton et al., 1999	CK6	LEW 87009	-4.32	Clayton et al., 1999
CM1	EET 83334	-2.28	Clayton et al., 1999	CO3	Isna	-4.55	Clayton et al., 1999	CR1	GRO 95577	-0.45	Clayton et al., 1999
CM1/2	ALH 83100	-2.50	Clayton et al., 1999	CO3	Kainsaz	-4.72	Clayton et al., 1999	CR2	Al Rais	-1.01	Clayton et al., 1999
CM1/2	Y 82042	-2.02	Clayton et al., 1999	CO3	Lance	-4.35	Clayton et al., 1999	CR2	EET 87770	-1.22	Clayton et al., 1999
CM2	A 881334	-4.16	Clayton et al., 1999	CO3	Ornans	-4.45	Clayton et al., 1999	CR2	Ei Djouf 001	-1.47	Clayton et al., 1999
CM2	A 881594	-2.49	Clayton et al., 1999	CO3	Warrenton	-4.07	Clayton et al., 1999	CR2	MAC 87320	-1.80	Clayton et al., 1999
CM2	A 881655	-2.37	Clayton et al., 1999	CO3	Y 791717	-4.37	Clayton et al., 1999	CR2	Renazzo	-0.96	Clayton et al., 1999
CM2	A 881955	-2.58	Clayton et al., 1999	CV3	Acfer 082	-3.73	Clayton et al., 1999	CR2	Y 790112	-1.56	Clayton et al., 1999
CM2	Banten	-2.97	Clayton et al., 1999	CV3	Acfer 086	-3.40	Clayton et al., 1999	CR2	Y 791498	-1.64	Clayton et al., 1999
CM2	Cimarron	-2.91	Clayton et al., 1999	CV3	Acfer 272	-2.65	Clayton et al., 1999	CR2	Y 793495	-1.63	Clayton et al., 1999
CM2	Cold Bokkeveld	-2.45	Clayton et al., 1999	CV3	Allende	-3.52	Clayton et al., 1999	CR2	Y 8449	-2.16	Clayton et al., 1999
CM2	EET 87522	-3.71	Clayton et al., 1999	CV3	Axtell	-3.35	Clayton et al., 1999	CH3	Acfer 182	-1.55	Clayton et al., 1999
CM2	LEW 85311	-3.23	Clayton et al., 1999	CV3	Ningqiang	-4.55	Clayton et al., 1999	CH3	ALH 85085	-1.62	Clayton et al., 1999
CM2	LEW 87016	-2.95	Clayton et al., 1999	CV3	Tibooburra	-4.71	Clayton et al., 1999	CH3	PAT 91546	-1.25	Clayton et al., 1999
CM2	LEW 87022	-2.20	Clayton et al., 1999	CV3	Bali	-2.48	Clayton et al., 1999	CH3	PCA 91328	-1.50	Clayton et al., 1999
CM2	LEW 87148	-2.15	Clayton et al., 1999	CV3	Bali	-4.90	Clayton et al., 1999	CH3	PCA 91452	-1.27	Clayton et al., 1999
CM2	LEW 88001	-2.90	Clayton et al., 1999	CV3	Grosnaja	-3.13	Clayton et al., 1999	CH3	PCA 91467	-1.47	Clayton et al., 1999
CM2	LEW 88002	-4.21	Clayton et al., 1999	CV3	Kaba	-3.50	Clayton et al., 1999	CH3	RKP 92435	-1.52	Clayton et al., 1999
CM2	LEW 90500	-2.48	Clayton et al., 1999	CV3	Mokoia	-2.74	Clayton et al., 1999	CB	Bencubbin	-2.27	Weisberg et al., 2001
CM2	MAC 88100	-2.13	Clayton et al., 1999	CV3	Arch	-4.95	Clayton et al., 1999	CB	Weatherford	-2.53	Weisberg et al., 2001
CM2	MAC 88101	-2.24	Clayton et al., 1999	CV3	Efremovka	-5.08	Clayton et al., 1999	CB	HH 237	-2.17	Weisberg et al., 2001
CM2	MAC 88176	-2.03	Clayton et al., 1999	CV3	Leoville	-5.87	Clayton et al., 1999	CB	QUE 94411	-2.25	Weisberg et al., 2001
CM2	Mighei	-2.50	Clayton et al., 1999	CV3	Leoville	-3.59	Clayton et al., 1999	C1/2-un	Y 82162	0.38	Clayton et al., 1999
CM2	Murchison	-2.60	Clayton et al., 1999	CV3	QUE 93429	-5.27	Clayton et al., 1999	C2 un	Acfer 094	-4.52	Clayton et al., 1999
CM2	Murray	-3.07	Clayton et al., 1999	CV3	Vigarano	-4.23	Clayton et al., 1999	C2 un	Adelaide	-3.62	Clayton et al., 1999
CM2	Nogoya	-2.00	Clayton et al., 1999	CK3	DG005	-4.12	Clayton et al., 1999	C2-un	B 7904	-0.05	Clayton et al., 1999
CM2	QUE 93005	-2.54	Clayton et al., 1999	CK3	Watson 002	-3.21	Clayton et al., 1999	C2-un	Bells	-1.86	Clayton et al., 1999
CM2	Y 793321	-2.94	Clayton et al., 1999	CK4	ALH 82135	-4.17	Clayton et al., 1999	C2-un	Essebi	-1.04	Clayton et al., 1999
CM2	Y 793595	-2.45	Clayton et al., 1999	CK4	Karoonda	-4.48	Clayton et al., 1999	C2 un	GRO 95566	-3.97	Clayton et al., 1999
CM2	Y 82054	-4.84	Clayton et al., 1999	CK4	LEW 86258	-4.55	Clayton et al., 1999	C2 un	MAC 87300	-3.95	Clayton et al., 1999
CM2	Y 82098	-3.81	Clayton et al., 1999	CK4	LEW 87214	-4.25	Clayton et al., 1999	C2 un	MAC 88107	-4.39	Clayton et al., 1999
CM2	Y 86695	-4.14	Clayton et al., 1999	CK4	Maralinga	-4.45	Clayton et al., 1999	C2-un	Y 86720	-0.01	Clayton et al., 1999
CO3	Acfer 202	-4.00	Clayton et al., 1999	CK4	PCA 82500	-3.46	Clayton et al., 1999	C2-un	Y 86789	-0.06	Clayton et al., 1999
CO3	Acfer 243	-4.26	Clayton et al., 1999	CK4	Y 6903	-4.17	Clayton et al., 1999	C3-un	LEW 85332	-2.42	Clayton et al., 1999
CO3	ALH 77307	-4.47	Clayton et al., 1999	CK5	EET 83311	-4.32	Clayton et al., 1999	C4-un	Coolidge	-4.50	Clayton et al., 1999
CO3	DaG 006	-3.88	Clayton et al., 1999	CK5	EET 87507	-4.15	Clayton et al., 1999	C4-un	HH 073	-3.76	Clayton et al., 1999
CO3	DaG 023	-4.33	Clayton et al., 1999	CK5	EET 87860	-4.14	Clayton et al., 1999	Average with 95% confidence		-3.01 ± 0.26	

Table S2. (continued)

Class	Sample	$\Delta^{17}\text{O}$	Reference	Class	Sample	$\Delta^{17}\text{O}$	Reference	Class	Sample	$\Delta^{17}\text{O}$	Reference
Ordinary chondrite											
H4	Bath	0.71	Clayton et al., 1991	L5	Elenovka	1.16	Clayton et al., 1991	LL6	Ensisheim	1.40	Clayton et al., 1991
H4	Beaver creek	0.76	Clayton et al., 1991	L5	Elenovka	0.97	Clayton et al., 1991	LL6	Jelica	1.27	Clayton et al., 1991
H4	Forest Vale	0.74	Clayton et al., 1991	L5	Ergheo	0.98	Clayton et al., 1991	LL6	Mangwandi	1.14	Clayton et al., 1991
H4	Forest Vale	0.53	Clayton et al., 1991	L5	Farmington	1.13	Clayton et al., 1991	LL6	St. Mesmin	1.13	Clayton et al., 1991
H4	Kesen	0.63	Clayton et al., 1991	L5	Homestead	1.11	Clayton et al., 1991	LL6	St. Séveron	1.16	Clayton et al., 1991
H4	Ochansk	0.82	Clayton et al., 1991	L5	Knyahinya	1.05	Clayton et al., 1991	LL6	Vavilovka	1.21	Clayton et al., 1991
H4	Tysnes Island	0.70	Clayton et al., 1991	L5	Qidong	1.09	Clayton et al., 1991	Average with 95% confidence			1.01 ± 0.05
H4	Weston	0.88	Clayton et al., 1991	L6	Bachmut	1.16	Clayton et al., 1991	Enstatite chondrite			
H5	Allegan	0.63	Clayton et al., 1991	L6	Barwell	1.19	Clayton et al., 1991	EH3	Qingzhen	-0.03	Clayton et al., 1984
H5	Allegan	0.59	Clayton et al., 1991	L6	Barwell	1.14	Clayton et al., 1991	EH4	Adhi Kot	-0.05	Clayton et al., 1984
H5	Ambapur Nagla	0.75	Clayton et al., 1991	L6	Bori	1.06	Clayton et al., 1991	EH4	Indarch	0.12	Clayton et al., 1984
H5	Beardsley	0.75	Clayton et al., 1991	L6	Cabezo de Mayo	1.04	Clayton et al., 1991	EH4	Kota Kota	-0.15	Clayton et al., 1984
H5	Forest City	0.75	Clayton et al., 1991	L6	Mocs	1.13	Clayton et al., 1991	EH4	Parsa	0.01	Clayton et al., 1984
H5	Leighton	0.87	Clayton et al., 1991	L6	Modoc	1.08	Clayton et al., 1991	EH4	Parsa	0.05	Clayton et al., 1984
H5	Pantar	0.56	Clayton et al., 1991	L6	Ramsdof	0.83	Clayton et al., 1991	EH4	South Oman	-0.37	Clayton et al., 1984
H5	Richardton	0.64	Clayton et al., 1991	L6	Ramsdof	0.78	Clayton et al., 1991	EH4	Y691	-0.05	Clayton et al., 1984
H5	Richardton	0.58	Clayton et al., 1991	L6	Tathlith	1.15	Clayton et al., 1991	EH5	St.Marks	0.11	Clayton et al., 1984
H5	Xingyang	0.81	Clayton et al., 1991	L6	Tillaberi	0.97	Clayton et al., 1991	EH5	St. Sauveur	0.04	Clayton et al., 1984
H5	Zhovtnevyi	0.86	Clayton et al., 1991	L6	Xiujimgin	1.06	Clayton et al., 1991	EL6	Atlanta	0.03	Clayton et al., 1984
H6	Cape Girardeau	0.72	Clayton et al., 1991	LL4	Albareto	1.20	Clayton et al., 1991	EL6	Blithfield	0.07	Clayton et al., 1984
H6	Charsonville	0.65	Clayton et al., 1991	LL4	Bo Xian	1.15	Clayton et al., 1991	EL6	Daniel's Kuil	0.00	Clayton et al., 1984
H6	Guarena	0.76	Clayton et al., 1991	LL4	Harnler	1.36	Clayton et al., 1991	EL6	Hvittis	0.07	Clayton et al., 1984
H6	Kernouve	0.78	Clayton et al., 1991	LL4	Savtschenskoje	1.18	Clayton et al., 1991	EL6	Jajh deh Kot Lalu	0.07	Clayton et al., 1984
H6	Mt. Browne	0.69	Clayton et al., 1991	LL4	Savtschenskoje	1.39	Clayton et al., 1991	EL6	Khairpur	0.10	Clayton et al., 1984
H6	Queen's Mercy	0.72	Clayton et al., 1991	LL4	Soko Banja	1.32	Clayton et al., 1991	EL6	Pillistfer	0.02	Clayton et al., 1984
L4	Atarra	1.14	Clayton et al., 1991	LL4	Witsand Farm	1.35	Clayton et al., 1991	EL6	Ufana	0.12	Clayton et al., 1984
L4	Bjurbole	1.00	Clayton et al., 1991	LL5	Guidder	1.19	Clayton et al., 1991	Average with 95% confidence			0.01 ± 0.06
L4	Cynthiana	1.08	Clayton et al., 1991	LL5	Khanpur	1.41	Clayton et al., 1991	SNC			
L4	Kendleton	1.03	Clayton et al., 1991	LL5	Olivernza	1.14	Clayton et al., 1991	shergottite	Shergotty	0.70	Clayton et al., 1983
L4	Nan Yang Po	0.97	Clayton et al., 1991	LL5	Olivernza	1.11	Clayton et al., 1991	shergottite	Zagami	0.80	Clayton et al., 1983
L4	Saratov	1.02	Clayton et al., 1991	LL5	Paragould	1.39	Clayton et al., 1991	naxhlite	Nakhla	0.50	Clayton et al., 1983
L4	Tennasilml	1.15	Clayton et al., 1991	LL5	Siena	1.32	Clayton et al., 1991	naxhlite	Lafayette	0.62	Clayton et al., 1983
L5	Ausson	1.12	Clayton et al., 1991	LL6	Appley Bridge	1.32	Clayton et al., 1991	chassignite	Chassigny	0.62	Clayton et al., 1983
L5	Ausson	1.16	Clayton et al., 1991	LL6	Appley Bridge	1.27	Clayton et al., 1991	Average with 95% confidence			0.65 ± 0.15
L5	Borkut	1.06	Clayton et al., 1991	LL6	Dhurmsala	1.15	Clayton et al., 1991				
L5	Chervettaz	1.25	Clayton et al., 1991	LL6	Dongtai	1.02	Clayton et al., 1991				

Table S3. ^{54}Cr isotopic compositions in chondrites and Martian meteorites from previous work.

Class	Sample	$\epsilon^{54}\text{Cr}$	95% Conf.	Reference	Class	Sample	$\epsilon^{54}\text{Cr}$	95% Conf.	Reference
Carbonaceous chondrites					Enstatite chondrites				
CI	Orgueil	1.55	0.13	Qin et al., 2010	EH3	ALHA 77295	0.05	0.14	Qin et al., 2010
CI	Orgueil	1.69	0.09	Qin et al., 2010	EH3	Kota Kota	-0.02	0.21	Trinquier et al., 2007
CI	Orgueil	1.56	0.06	Trinquier et al., 2007	EH3	Kota Kota	0.04	0.07	Trinquier et al., 2007
CM2	Murchison	0.97	0.20	Qin et al., 2010	EH3	Qingzhen	-0.02	0.08	Trinquier et al., 2007
CM2	Murchison	1.01	0.05	Trinquier et al., 2007	EH4	Indarch	0.05	0.14	Qin et al., 2010
CO3	Felix	0.63	0.09	Trinquier et al., 2007	EH4	Abee	-0.06	0.12	Trinquier et al., 2007
CO3	Kainsaz	0.87	0.18	Qin et al., 2010	EL3	MAC 88136	0.02	0.09	Qin et al., 2010
CO3	Lance	0.57	0.11	Trinquier et al., 2007	EL6	Hvittis	-0.01	0.17	Trinquier et al., 2007
CV3	Allende	0.98	0.14	Qin et al., 2010	EL6	LON 94100	-0.02	0.14	Qin et al., 2010
CV3	Allende	0.92	0.13	Qin et al., 2010	EL6	Pillistfer	0.09	0.08	Trinquier et al., 2007
CV3	Allende	0.86	0.09	Trinquier et al., 2007	Weighted average		0.02	0.03	
CV3	Leoville	0.71	0.15	Qin et al., 2010	MSWD		0.79		
CV3	Vigarano	0.91	0.12	Qin et al., 2010	SNC				
CV3	Vigarano	0.82	0.13	Qin et al., 2010		Nakhla	-0.21	0.16	Qin et al., 2010
CK4	Karoonda	0.63	0.09	Trinquier et al., 2007		Shergotty	-0.18	0.17	Trinquier et al., 2007
CR2	GRA 06100	1.32	0.11	Qin et al., 2010		Chassigny	-0.20	0.05	Trinquier et al., 2007
CR2	Renazzo	1.30	0.21	Trinquier et al., 2007		Nakhla	-0.14	0.08	Trinquier et al., 2007
CB	Bencubbin	1.11	0.09	Trinquier et al., 2007	Weighted average		-0.19	0.04	
CB	Bencubbin	1.13	0.09	Trinquier et al., 2007	MSWD		0.58		
Weighted average		1.03	0.15		Weighted average		-0.19	0.04	
MSWD		50*			MSWD		0.58		
Ordinary chondrites									
H4	Ste Marguerite	-0.39	0.07	Trinquier et al., 2007					
H4	LAP 03601	-0.28	0.11	Qin et al., 2010					
H6	Kernouvé	-0.37	0.08	Trinquier et al., 2007					
L3	QUE 97008	-0.42	0.14	Qin et al., 2010					
LL3.4	Chainpur	-0.47	0.07	Trinquier et al., 2007					
LL4	GRO 95552	-0.33	0.10	Qin et al., 2010					
LL6	Saint Severin	-0.41	0.10	Trinquier et al., 2007					
LL6	Saint Severin	-0.42	0.03	Trinquier et al., 2007					
Weighted average		-0.41	0.04						
MSWD		1.8							

* See the footnote of Table S1.

Table S4. ^{50}Ti isotopic compositions in chondrites and Martian meteorites from previous work..

Class	Sample	$\epsilon^{50}\text{Ti}$	95% Conf.	Reference	Class	Sample	$\epsilon^{50}\text{Ti}$	95% Conf.	Reference
Carbonaceous chondrites					Ordinary chondrites				
CI	Orgueil	1.92	0.27	Trinquier et al., 2009	H4	Kesen	-0.37	0.05	Zhang et al., 2012
CI	Orgueil	1.86	0.11	Trinquier et al., 2009	H5	Juancheng	-0.66	0.16	Trinquier et al., 2009
CI	Orgueil	1.74	0.05	Zhang et al., 2012	H6	St-severin	-0.74	0.20	Trinquier et al., 2009
CM2	Murchison	3.32	0.16	Trinquier et al., 2009	L3.7	Hedjaz	-0.65	0.13	Trinquier et al., 2009
CM2	Murchison	3.06	0.33	Trinquier et al., 2009	L5	Ausson	-0.64	0.03	Zhang et al., 2012
CM2	Murchison	3.15	0.05	Trinquier et al., 2009	L6	Isoulane-n-Amahar	-0.59	0.05	Zhang et al., 2012
CM2	Murchison	2.96	0.07	Trinquier et al., 2009	LL3	Dar al Gani	-0.72	0.16	Trinquier et al., 2009
CM2	Murchison	3.19	0.11	Trinquier et al., 2009	LL3.2	Krymka	-0.66	0.05	Zhang et al., 2012
CM2	Murchison	2.94	0.06	Trinquier et al., 2009	LL5	Paragould	-0.61	0.07	Zhang et al., 2012
CM2	Murchison	3.08	0.05	Trinquier et al., 2009	Un 3	NWA5717	-0.58	0.05	Zhang et al., 2012
CM2	Murray	2.84	0.05	Zhang et al., 2012	Un 3	NWA5717	-0.63	0.05	Zhang et al., 2012
CO3	Isna	3.45	0.23	Trinquier et al., 2009	Weight average		-0.61	0.06	
CO3	Lance	3.46	0.10	Zhang et al., 2012	MSWD		10.5*		
CO3	Ornans	3.37	0.09	Zhang et al., 2012	Enstatite chondrites				
CV3	Allende	4.98	0.29	Trinquier et al., 2009	EH3	Qingzhen	0.02	0.12	Trinquier et al., 2009
CV3	Allende	5.01	0.29	Trinquier et al., 2009	EH3	Qingzhen	-0.26	0.32	Trinquier et al., 2009
CV3	Allende	3.49	0.04	Zhang et al., 2012	EH3	Sahara 97072	-0.15	0.06	Zhang et al., 2012
CV3	Leoville	4.09	0.08	Zhang et al., 2012	EH4	Indarch	-0.13	0.05	Zhang et al., 2012
CK4	Karoonda	3.26	0.10	Zhang et al., 2012	EH4	Adhi Kot	-0.10	0.04	Zhang et al., 2012
CR2	NWA 801	2.35	0.04	Zhang et al., 2012	EH4	Abee	-0.06	0.04	Zhang et al., 2012
CR2	Sahara 0082	2.60	0.30	Trinquier et al., 2009	EH4	Abee	-0.06	0.04	Zhang et al., 2012
Weight average		3.15	0.36		EH5	Saint-Sauveur	-0.15	0.09	Zhang et al., 2012
MSWD		301*			EL6	Hvittis	-0.29	0.07	Zhang et al., 2012
Martian meteorite					EL6	Jajh deh Kot Lalu	-0.29	0.10	Zhang et al., 2012
SNC		-0.31	0.17	Trinquier et al., 2009	Weight average		-0.15	0.07	
NWA 2737		-0.31	0.17	Trinquier et al., 2009	MSWD		6.6*		

* See the footnote of Table S1.

Table S5. ^{92}Mo isotopic compositions in chondrites and Martian meteorites from previous work.

Class	Sample	$\epsilon^{92}\text{Mo}$	95% Conf.	Reference
Carbonaceous chondrites				
CI	Orgueil	1.12	0.59	Burkhardt et al. 2011
CI	Orgueil	0.53	0.57	Dauphas et al., 2002
CM2	Murchison	6.34	1.31	Burkhardt et al. 2011
CM2	Murchison	6.66	0.53	Burkhardt et al. 2011
CM2	Murchison	6.36	0.55	Burkhardt et al. 2011
CO3	NWA2090	1.48	0.53	Burkhardt et al. 2011
CV3	Allende	3.24	0.86	Burkhardt et al. 2011
CV3	Allende	3.46	0.51	Burkhardt et al. 2011
CV3	Allende	2.38	0.57	Dauphas et al., 2002
CV3	Allende	3.54	0.67	Dauphas et al., 2002
CV3	Allende	2.57	0.78	Dauphas et al., 2002
CV3	Allende	1.23	0.39	Dauphas et al., 2002
CR2	NWA801	3.58	0.64	Burkhardt et al. 2011
Weighted average		3.20	1.10	
MSWD		51*		
Ordinary chondrites				
H3	Bremervorde	0.72	0.53	Burkhardt et al. 2011
H6	Kernouvé	0.66	0.59	Burkhardt et al. 2011
Weighted average		0.69	0.39	
MSWD		0.023		
Enstatite chondrites				
EH4	Abee	0.65	1.11	Burkhardt et al. 2011
EH4	Abee	0.36	0.26	Burkhardt et al. 2011
EH4	Indarch	-0.44	1.25	Dauphas et al., 2002
EH4	Indarch	0.88	0.86	Dauphas et al., 2002
EH4	Saint Sauveur	0.15	0.62	Dauphas et al., 2002
EH4	Saint Sauveur	0.09	1.86	Dauphas et al., 2002
EL6	Pilistfer	-1.03	0.94	Dauphas et al., 2002
EL6	Pilistfer	1.04	1.15	Dauphas et al., 2002
Weighted average		0.30	0.35	
MSWD		2.0		
Martian meteorites				
	Zagami	0.52	0.75	Burkhardt et al. 2011
	DaG476	-0.12	0.75	Burkhardt et al. 2011
Weighted average		0.20	0.75	
MSWD		1.5		

* See the footnote of Table S1.